Received: 19 September 2024 | Revised: 17 January 2025 | Accepted: 31 January 2025

DOI: 10.1002/alz.70060

Alzheimer's & Dementia®
THE JOURNAL OF THE ALZHEIMER'S ASSOCIATION

RESEARCH ARTICLE

Metabolic stress and age drive inflammation and cognitive decline in mice and humans

Sarah E. Elzinga[1,8] | Kai Guo[1] | Ali Turfah[2] | Rosemary E. Henn[1] | Ian F. Webber-Davis[1] | John M. Hayes[1] | Crystal M. Pacut[1] | Samuel J. Teener[1] | Andrew D. Carter[1] | Diana M. Rigan[1] | Adam M. Allouch[1] | Dae-Gyu Jang[1] | Rachel Parent[3] | Emily Glass[4] | Geoffrey G. Murphy[4] | Stephen I. Lentz[5] | Kevin S. Chen[1,6] | Lili Zhao[2] | Junguk Hur[7] | Eva L. Feldman[1]

[1]Department of Neurology, University of Michigan, Ann Arbor, Michigan, USA

[2]Department of Biostatistics, School of Public Health, University of Michigan, Ann Arbor, Michigan, USA

[3]Department of Internal Medicine, General Medicine, University of Michigan, Ann Arbor, Michigan, USA

[4]Department of Molecular and Integrative Physiology, Division of Cardiovascular Medicine, University of Michigan, Ann Arbor, Michigan, USA

[5]Department of Internal Medicine, Division of Metabolism, Endocrinology, and Diabetes, University of Michigan, Ann Arbor, Michigan, USA

[6]Department of Neurosurgery, University of Michigan, Ann Arbor, Michigan, USA

[7]Department of Biomedical Sciences, University of North Dakota, Grand Forks, North Dakota, USA

[8]Department of Physiology, Michigan State University, East Lansing, Michigan, USA

Correspondence
Sarah E. Elzinga, Department of Physiology, Michigan State University, 2201 Biomedical and Physical Sciences, 567 Wilson Road, East Lansing, MI 48824, USA.
Email: seelzing@med.umich.edu

Abstract

INTRODUCTION: Metabolic stressors (obesity, metabolic syndrome, prediabetes, and type 2 diabetes [T2D]) increase the risk of cognitive impairment (CI), including Alzheimer's disease (AD). Immune system dysregulation and inflammation, particularly microglial mediated, may underlie this risk, but mechanisms remain unclear.

METHODS: Using a high-fat diet-fed (HFD) model, we assessed longitudinal metabolism and cognition, and terminal inflammation and brain spatial transcriptomics. Additionally, we performed hippocampal spatial transcriptomics and single-cell RNA sequencing of *post mortem* tissue from AD and T2D human subjects versus controls.

Sarah E. Elzinga and Kai Guo contributed equally.

Funding information: Cure PSP (AD Knowledge Portal); Arizona Department of Health Services and the Arizona Biomedical Research Commission (AD Knowledge Portal); National Institutes of Health, Grant/Award Numbers: K99AG071667, R01DK130913, P30EY007003, P30DK020572, P30AG053760, P30AG072931, S10OD28612-01-A1, P30CA046592; Alzheimer's Association, Grant/Award Number: AACSF-22-970586; Robert E. Nederlander Sr. Program for Alzheimer's Research; Andrea and Lawrence A. Wolfe Brain Health Initiative; Frank L. and Helen Gofrank Foundation Research Program in Alzheimer's Disease and Brain Health; Kiriluk Family Fund for Brain Health Research; Robert and Katherine Jacobs Environmental Health Initiative; Sinai Medical Staff Foundation Research on Studying Diet and Brain Health Fund; Kenneth and Frances Eisenberg Emerging Scholar Fund; Edith S. Briskin/SKS Foundation NeuroNetwork Emerging Scholar Fund; Handleman Emerging Scholar Fund; Tauber Family Student Internship Program; Taubman Foundation; NeuroNetwork for Emerging Therapies; National Institutes of Health (AD Knowledge Portal), Grant/Award Numbers: P30AG10161, P30AG72975, R01AG15819, R01AG17917, R01AG036836, U01AG46152, U01AG61356, U01AG046139, P50AG016574, R01AG032990, R01AG018023, U01AG006576, U01AG006786, R01AG025711, R01AG017216, R01AG003949, R01NS080820, U24NS072026, P30AG19610, U01AG046170, RF1AG057440, U24AG061340; Mayo and Michael J. Fox Foundations (AD Knowledge Portal)

RESULTS: HFD induced progressive metabolic and CI with terminal inflammatory changes, and dysmetabolic, neurodegenerative, and inflammatory gene expression profiles, particularly in microglia. AD and T2D human subjects had similar gene expression changes, including in secreted phosphoprotein 1 (*SPP1*), a pro-inflammatory gene associated with AD.

DISCUSSION: These data show that metabolic stressors cause early and progressive CI, with inflammatory changes that promote disease. They also indicate a role for microglia, particularly microglial *SPP1*, in CI.

KEYWORDS
cognitive impairment, hippocampus, human, inflammation, microglia, mouse, obesity, prediabetes, type 2 diabetes

Highlights

- Metabolic stress causes persistent metabolic and cognitive impairments in mice.
- Murine and human brain spatial transcriptomics align and indicate a pro-inflammatory milieu.
- Transcriptomic data indicate a role for microglial-mediated inflammatory mechanisms.
- Secreted phosphoprotein 1 emerged as a potential target of interest in metabolically driven cognitive impairment.

1 | BACKGROUND

The aging population is growing worldwide with a tandem rise in cognitive impairment (CI), including dementias such as Alzheimer's disease (AD) and related dementias (ADRD).[1,2] In parallel, increasing rates of metabolic stressors, including obesity,[3] prediabetes, metabolic syndrome, and type 2 diabetes (T2D),[4,5] which are CI risk factors, further inflate this burden.[6–8] However, treatment options are limited, likely due to insufficiently targeted interventions administered too late in the disease course to halt or reverse progression.

Inflammation and immune system dysregulation are shared etiologies underlying obesity, prediabetes, metabolic syndrome, T2D, and CI.[9–11] Complex and highly regulated, when aberrantly or constitutively activated the immune system can contribute to neurodegeneration,[12,13] ultimately leading to CI. Indeed, the timeline of immune system activation and its resolution can be altered in disease states.[12] However, associated cognitive effects of this immune dysregulation are not well understood. This is particularly relevant because it is critical to identify not only therapeutic targets, but also appropriate therapeutic windows for treatment.

Several specific inflammatory or immune pathways are implicated in the pathogenesis of CI,[13] including Toll-like receptor 4,[14] nuclear factor kappa B (NFκB),[15] and the inflammasome,[16] all commonly dysregulated in the brain during metabolic stress and neurodegenerative diseases, including AD/ADRD. Inflammatory pathways are highly expressed in microglia,[17,18] including secreted phosphoprotein 1 (SPP1), which has recently emerged as a potentially critical inflammatory pathway in AD/ADRD.[19,20] As the resident central nervous system (CNS) immune cells, microglia are proposed to play a pivotal role in the progression of CI.[21–23] Activated in metabolic stress and AD/ADRD, microglia adopt a pro-inflammatory phenotype with altered morphology and inflammatory cytokine production.[24–28] Despite their prominent role, there is no consensus in the field regarding specific immune or inflammatory pathways which predominantly contribute to disease, nor the participation of other cell-specific mechanisms.

To gain a deeper understanding, we longitudinally analyzed metabolic and cognitive changes in a mouse model of obesity, prediabetes, and CI. At the study end, we assessed inflammatory measures and spatially relevant changes in brain gene expression. To identify translationally relevant targets, we also assessed spatial and cell-specific changes in gene expression in hippocampi from human subjects with AD and T2D versus controls and compared our results to a larger existing bioinformatics human dataset from the AD Knowledge Portal (specifically Accelerating Medicines Partnership–Alzheimer's Disease [AMP-AD] data). Finally, we associated changes in murine gene expression and microglial morphology with cognitive outcomes, highlighting the translational, cell-specific, and physiological relevance of our work.

2 | METHODS

2.1 | Animals

Six-week-old C57BL6 diet-induced obesity (DIO) mice (380050) and C57BL6 controls (380056) were purchased from Jackson Laboratories. Animals were fed either 60% HFD (high-fat diet, D12492) or 10% SD (standard diet, D12450H) from Research Diets for the duration of the experiment. Animals were housed in the University of Michigan's facilities in a pathogen-free room with ad libitum access to food and water. Housing conditions were maintained per the University of Michigan Unit for Laboratory Animal Medicine's standard protocols, that is, 20 ± 2°C, 12 hour light/dark cycle, and minimum of one enrichment item per cage. At the study end, animals were either given an intraperitoneal injection of 260 µg/kg body weight (BW) lipopolysaccharide (LPS) dissolved in saline or saline alone as a control 4 hours prior to sacrifice. Animals were monitored daily by staff and all experimental procedures were approved by the University of Michigan's Institutional Animal Care and Use Committee (PRO0010039).

2.2 | *Post mortem* human hippocampal samples

In collaboration with the Michigan Alzheimer's Disease Research Center, $n = 6$ human formalin fixed paraffin embedded (FFPE) blocks containing hippocampal samples ($n = 3$ control and $n = 3$ AD+T2D subjects) were obtained through the Michigan Brain Bank in collaboration with the Michigan Alzheimer's Disease Research Center. All Michigan Brain Bank living participants complete a donation preregistration consent form which allows for collection of demographic and medical record information needed to complete the registration process. The Michigan Brain Bank obtains a verbal consent for autopsy from the participant's next of kin through our Michigan Medicine autopsy consent line. Consents are completely voluntary; participants and next of kin are welcome to withdraw at any time.

2.3 | Metabolic phenotyping

Metabolic phenotyping consisted of periodic BWs (approximately weekly) and glucose tolerance testing (GTT; approximately every 2 months). GTTs were performed as previously published.[29,30] At terminal, additional phenotyping consisted of fasting insulin levels, liver pathology, and adipocyte hypertrophy. Insulin levels in plasma were measured via enzyme-linked immunosorbent assay (ELISA) by the University of Michigan's Metabolic, Physiological and Behavioral Phenotyping Core. Liver pathology was performed by the University of Michigan Unit for Laboratory Animal Medicine Pathology Core. Adipocyte hypertrophy was measured using hematoxylin and eosin staining, followed by imaging, and analysis via MetaMorph software, as previously published.[31]

RESEARCH IN CONTEXT

1. **Systematic review**: Using sources from PubMed and Google Scholar, including published articles, abstracts, and presentations, the authors thoroughly reviewed the literature. Alzheimer's disease (AD) is extensively studied (and appropriately cited in the manuscript). However, the contribution of metabolic stressors (obesity, metabolic syndrome, prediabetes, and type 2 diabetes), and their resulting inflammation to cognitive impairments, such as AD, remains incompletely understood.
2. **Interpretation**: We find that microglia play an important role in promoting cognitive impairment under conditions of metabolic stress, which is exacerbated with aging in both mice and humans. Our data also indicate that secreted phosphoprotein 1 (SPP1) may present a potential therapeutic target for metabolically driven cognitive impairment.
3. **Future directions**: This article provides the preliminary data to explore translationally relevant inflammatory, microglial-specific therapeutic targets, including SPP1.

2.4 | Cognitive phenotyping

Cognition was assessed by Morris water maze (MWM) and puzzle box. MWM was performed after 1 month on diet using previously published methods.[32] In brief, animals underwent 9 days of training with four trials per day in which they had a maximum of 60 seconds to locate a platform hidden beneath the opaque surface of the water. Probe trials (60 seconds) during which the platform was removed were performed prior to training on days 4 and 7, as well as on the day after training ended (day 10). Additional probe trials were also performed after 2 and 12 months on diet. Puzzle box was performed after 6 months on diet, per previously published protocols,[24] and repeated after 8, 10, and 12 months on diet with slightly modified methods. In brief, animals were allowed a maximum of 5 minutes in the box to escape from the light area into the dark area. A series of increasingly complex single obstacles (each replicated for three trials) were placed in front of the opening from the light to dark areas and time to escape recorded. After single obstacle trials, all single obstacles were combined into one complex obstacle to measure time to escape. For repeated puzzle box tests, if a single obstacle had been previously used during a previous dietary time point (i.e., 6 vs. 8 months on diet), it was only replicated once for a total of two trials. Obstacles that were not previously used in prior dietary time points were replicated for the full three trials. Repeated complex obstacles were performed prior to any single obstacles (on day 1 of 3). After 10 and 12 months on diet, only the complex obstacles were performed, and all three different complex obstacles were performed only once.

2.5 | Inflammatory phenotyping

Inflammatory phenotypes were measured using ELISA for cytokines (from murine plasma and microglial cell lysate-microglial experiments described below) and hippocampal immunohistochemistry (IHC) for microglial activation using morphology. ELISAs were performed by the University of Michigan's Rogel Cancer Center Immunology Core for the inflammatory cytokines interferon beta (IFN-ß), interleukin 6 (IL-6), vascular endothelial growth factor (VEGF), monocyte chemoattractant protein-1 (MCP-1), and tumor necrosis factor alpha (TNF-α) in plasma and for IL-6, interferon gamma (IFN-γ), TNF-α, chemokine ligand 1 (CXCL1), matrix metalloproteinase 9 (MMP-9), IL-2, and granulocyte-marcophage colony-stimulating factor (GM-CSF) in cell lysates. Hippocampal microglial morphology was determined via ionized calcium-binding adapter molecule 1 (IBA1) staining of hippocampal tissue sections, confocal imaging, and MatLab analysis to measure multiple morphological characteristics, per previously published protocols.[24,30,33]

2.6 | Transcriptomics

Hemi-brains from $n = 3$ mice/group, plus an additional technical replicate for $n = 1$ mouse/group, were fresh frozen and stored at −80°C until sent to the University of Michigan Advanced Genomics Core for spatial transcriptomics analysis using the 10x Genomics Visium platform. FFPE blocks with human hippocampal samples ($n = 3$ control and $n = 3$ AD+T2D subjects) were also sent to the Advanced Genomics Core for spatial transcriptomics analysis using the 10x Genomics Visium platform and for single-cell RNA sequencing using the 10x Genomics Chromium platform.

2.7 | In vitro microglial experiments

A human microglial cell line (ABM cat# T0252) was cultured and treated with the saturated fatty acid palmitate as previously published.[24] In brief, cells were cultured until ≈ 80% confluent and then treated with 62.5 µM palmitate or bovine serum albumin control for 24 hours. After treatment, supernatant and cell lysates were collected for downstream analyses for markers of inflammation (via ELISA or quantitative polymerase chain reaction [qPCR]) and cell death (via luminescence). ELISA is detailed above, and qPCR and luminescence are detailed below.

2.8 | qPCR and apoptosis

qPCR was performed on fresh frozen hippocampal tissue, per previously published protocols[34] using the following TaqMan primer/probes (Thermo Fisher Scientific): Spp1 (Mm00436767_m1), App (Mm01344172_m1), Sema4 g (Mm00442518_m1), and yWhaz as a control (Mm03950126_s1). Apoptosis in cells was measured by caspase activity using a commercially available kit (Promega, cat# G8090), per the manufacturer's instructions.

2.9 | IHC and RNAscope

To validate our transcriptomics results and confirm changes in gene expression of our targets of interest in microglia, we performed IHC with subsequent RNAscope on fixed samples from our murine brains. Specifically, we used SD ($n = 4$ animals, $n = 2$ slides/animal) and HFD ($n = 4$, $n = 2$ slides/animal) mice given saline. Fourteen micron sections were first stained with IBA1 to identify microglia, as described above. Next, slides were probed for SPP1 and C1qa gene expression using RNAscope (ABCD Bio; SPP1 cat# 485361 and C1qa cat# 441221-C2), per the manufacturer's instructions. Slides were imaged on a Leica Stellaris confocal microscope using a 40x oil objective. Hippocampal images ($n = 2$ images in the molecular layer and $n = 1$ image in the hilus and CA1 regions) were analyzed using MetaMorph software where 150-pixel circles were drawn around IBA1-positive cells and the threshold feature was used to further isolate microglia and identify SPP1 and C1qa signal within microglia. Data were evaluated as percent area of total microglia for SPP1 and C1qa, averaged for each region between each animal's slides.

2.10 | Statistics

2.10.1 | Metabolic and inflammatory data

Metabolic and inflammatory data, along with RNAscope, and cell death were analyzed using Prism 9.0 (GraphPad) and SAS 9.4. Prism analyzed adipocyte hypertrophy by two-way analysis of variance. Alternatively, SAS 9.4 was used to analyze plasma insulin, liver pathology, plasma cytokines, and qPCR using the ProcMixed function with diet and treatment (LPS vs. saline) set as fixed effects and individual animal identifiers set as a random effect. Changes in microglial morphology were determined using SAS 9.4 with diet, treatment (LPS vs. saline), and region (hilus, CA1, and molecular layer) set as fixed effects. The number of cells was set as a random effect and the different morphological metrics analyzed using the ProcMixed function. Additionally, SAS 9.4 was used for the correlative analysis to compare gene expression, ranked behavior, and microglial morphology using the ProcCorr function. Statistical significance was considered $P < 0.05$ and trends $P < 0.10$.

2.10.2 | Cognitive analyses

Trajectory data from WaterMaze software (ActiMetrics) were used to segment trajectories and classify these segmented trajectories (or swimming paths) into search strategies, as previously published and using the publicly available software RODA (https://github.com/RodentDataAnalytics/mwm-ml-gen).[35,36] In brief, each swimming path was assigned a search strategy (numbered 1–9) based on increasing search complexity. For each trial, total time spent in the pool and time spent per search strategy were used to calculate a weighted search strategy score, based on the relative time spent per strategy and the search strategy number (1–9), wherein a higher weighted score

indicated more sophisticated searching strategies for that trial. For both differences in time to platform and in weighted search strategies, a piecewise linear mixed effect model was used to test for effects of diet across different spans of time, adjusting for training day, group (SD vs. HFD), and their interaction. A random intercept for each mouse was used to consider correlations between data measured on the same animal.

Kaplan–Meier curves were used to estimate the probability of puzzle box escape over time (i.e., survival analyses), for which escape was exit from the light to the dark area of the box. The log-rank test was used to estimate the differences in these probabilities between groups. A Cox proportional hazards model compared differences in escape times between diet groups, adjusting for puzzle box obstacle, time point, and obstacle replicate. Interactions between diet and month as well as diet and obstacle were found to be significant; therefore, the diet effect across different months and across different obstacles was considered.

Area under the curve (AUC) for longitudinal weight data was calculated for each mouse. Weight at study start was set as a baseline and used to calculate the AUC and AUC was calculated for each puzzle box date using all recorded weight measurements prior to that time point. This value was divided by the number of days since baseline to have comparable AUC values for different months. GTT AUC was calculated from blood glucose concentrations at the different time points (baseline, 15, 30, 60, and 120 minutes after intraperitoneal glucose injection), scaling by the number of measurements.

A Cox proportional hazards model was used to determine the predictive ability of weight and GTT AUCs on puzzle box escape times. The model was adjusted for obstacle;, however, only measurements from the first replicate were considered. The model was fit using the AUC data from a given month (e.g., March; 4 months on diet) to predict the escape times for all subsequent months (e.g., July, September, November; 8, 10, and 12 months on diet, respectively).

Concordance indices were calculated for weight GTT AUC to compare the predictive ability of these measurements for subsequent puzzle box performance. To calculate concordance indices, all possible pairs of animals were compared. The proportion of pairs for whom the animal with a smaller AUC had a shorter escape time equals the concordance index. A larger concordance index indicates higher predictive ability. All the above cognitive analyses were conducted in R (version 4.1.2). Statistical significance was considered $p < 0.05$ and trends $P < 0.10$.

2.10.3 | Transcriptomics mapping cell types from single-cell RNA sequencing

To identify cell types within the spatial transcriptomics data, we conducted a label transfer from mouse single-cell RNA sequencing (scRNA-seq) data[37] or our human single-cell data to our mouse and human spatial transcriptomics data to deconvolve individual spot data, individually. Initially, anchors were computed using the FindTransferAnchors function with default parameters, using pre-processed scRNA-seq data as the reference and spatial transcriptomics data as the query. Subsequently, spot-level predictions were generated using the TransferData function for all slices, classifying the query cells according to the reference scRNA-seq data cell type labels. Normalized prediction scores were calculated by summing the prediction scores for each scRNA-seq cluster across all spots and normalizing these sums to one.

2.10.4 | Differential expression analysis and functional enrichment analysis

Differential expression analysis for each cluster or cell type was performed using the "FindMarker" function between groups. Differentially expressed genes (DEGs) were identified (adjusted $P < 0.05$) and significant pathways were further analyzed through functional enrichment analysis for Kyoto Encyclopedia of Genes and Genomes (KEGG) pathways using the richR package (https://github.com/hurlab/richR). The significantly enriched pathways were identified based on adjusted $P < 0.05$.

2.10.5 | Cell–cell communication analysis with CellChat

CellChat[38] was used to model signaling interactions within identified clusters. Due to multiple sample slices, we adapted CellChat's functions to ascertain significant interactions. A CellChat object was instantiated for each slice, and interactions were evaluated independently. The probability of ligand–receptor communication was then extracted from each object. If an interaction was not detected within slices between clusters, its value was set to zero. Only interactions observed across all three slices underwent significance testing. An interaction was deemed significant if it achieved a P value of < 0.05 using the Wilcoxon test. Differences in the number or strength of interactions among cell clusters across the two groups were analyzed similarly. Finally, the signaling network was visualized to elucidate potential cluster–cluster communications within the tissue sections, and the significant ligand receptors were visualized in the tissue sections. To identify the cluster with significant changes in sending or receiving signals between different groups, we summarized the sending or receiving signals for each slice.

2.10.6 | Gene set variation analysis

The KEGG pathway activities at the single-cell or spot level were assessed using the single sample gene set enrichment score (ssGSEA), as implemented in the scGSVA package (https://github.com/guokai8/scGSVA). The Wilcoxon test was used to estimate the statistical significance of the pathway enrichment between groups.

2.10.7 | Human dataset comparison

To increase the power of our human bioinformatics dataset and to increase the translational relevance of our data to the larger population, we incorporated publicly available RNA sequencing data from the AD Knowledge Portal. Specifically, we used data from the AMP-AD study. RNA sequencing data were obtained from the AMP-AD database in RDS format. Each RDS file was loaded and converted into Seurat objects for downstream analysis. Metadata, including cell-level and individual-level annotations, were directly incorporated from the dataset and mapped to the Seurat object metadata. The analysis focused only on AD and control groups, which were filtered based on the metadata annotations. To address potential imbalances, we performed random downsampling, retaining 50% of the cells within each combination of AD outcome and subcellular class. Normalization was performed using the NormalizeData function in Seurat. The cell-type annotations were directly obtained from the metadata provided in the RDS files, without additional integration or reclassification; cells labeled as "OtherImmune" were excluded in downstream analysis. Differential expression analysis was conducted for "broadcellclasse" and "subcellclass" using Seurat's FindMarkers function, comparing AD and control groups. Enrichment analysis of significantly altered genes was performed using the richR package to identify pathways associated with AD. Cell–cell communication networks were constructed separately for AD and control groups using the CellChat R package, which identifies overexpressed genes and interactions, computes communication probabilities, and aggregates signaling pathways. Then, the AD and control networks were merged for comparative analysis of signaling pathways and communication patterns.

3 | RESULTS

3.1 | HFD causes progressive metabolic stress

As expected, HFD progressively increased BW and impaired glucose tolerance (Figure 1A-E) and HFD mice had higher terminal plasma insulin levels versus SD animals (Figure S1A in supporting information). Immune challenge via LPS injection also increased plasma insulin levels compared to animals given saline; however, there was no additive effect of diet and LPS. We observed differences in adipocyte hypertrophy due to HFD (Figure S1B-E), but not in liver pathology (Figure S1F-H). Specifically, HFD versus SD saline mice had a reduced percentage of smaller adipocytes (Figure S1B). LPS also affected adipocyte hypertrophy, mostly in HFD animals, increasing the percentage of smaller adipocytes (Figure S1E). Together, these data indicate that HFD causes rapid weight gain and glucose intolerance, with corresponding increases in plasma insulin levels and adipocyte hypertrophy.

3.2 | HFD causes progressive CI

Cognition was assessed longitudinally using multiple methods (Figure 1A). After 6 months on diet, we found robust differences between HFD and SD groups using a puzzle box (Figure 2A-D), a task in mice that (while not brain region specific) primarily measures executive functioning.[39] Specifically, HFD animals were consistently slower to escape from the light area of the puzzle box to the dark area and were even often unable to complete the task. Deficits in puzzle box performance in HFD mice grew progressively more pronounced so that at the final time point, HFD animals were 4.68 times less likely to escape the light area of the box versus their SD counterparts (Figure S2 in supporting information). These results show that, similar to humans with CI and in humans with aging,[40] HFD causes deficits in executive functioning.

We and others have previously shown differences due to HFD by MWM,[41,42] a hippocampal-dependent task measuring spatial navigation and reference memory. Here, acutely, after 1 month on diet, HFD mice had a longer latency to reach the platform on day 2 of training (Figure S3 in supporting information), suggesting a delayed learning curve. Latencies do not take swimming paths into consideration and thus are not as sensitive to gradual changes in learning behavior over time.[35] Therefore, we further assessed potential diet-induced changes in search strategies to find the hidden platform,[35] but found no differences (Figures S4 andS5 in supporting information). A reduced latency to platform on day 2 of training (indicative of a slower learning curve), but not other differences in MWM data, were likely due to the acute timepoint (1 month on diet vs. 6+ months on diet for puzzle box data) and high individual variability between animals.

To understand the relationship between longitudinal cognitive outcomes and metabolic measures, we used Cox proportional hazards modeling and concordance indices. Cox proportional hazards evaluates if BW or GTT AUC influenced puzzle box escape times, whereas concordance indices quantify how well a model ranks subjects according to their risk, specifically the risk of AUCs on puzzle box escape times. Using both methods, we found that AUC for BW (calculation method; Figure S6 in supporting information) and GTT (Table S1, Figure S7 in supporting information) were predictive of future puzzle box performance. A lower hazard ratio and higher concordance index indicate a greater association with or predictability for puzzle box outcomes. Both models showed strengthened associations or predictions with a longer diet duration. Of interest, BW appeared to slightly outperform GTT regarding predicting cognitive performance with a higher concordance index at all time points.

3.3 | Chronic HFD alters peripheral and central inflammatory responses

At the study end, we assessed both peripheral (Figure S8 in supporting information) and CNS inflammatory responses (Figures S9, S10 in supporting information). In HFD mice, LPS stimulation differentially impacted plasma TNF-α: HFD mice had a blunted response (Figure S8A). Conversely, LPS increased circulating IL-6 and MCP-1 in SD and HFD mice to the same extent (Figure S8B,D). There was no effect of LPS or HFD on plasma IFN-β or VEGF concentrations (Figure S8C,E).

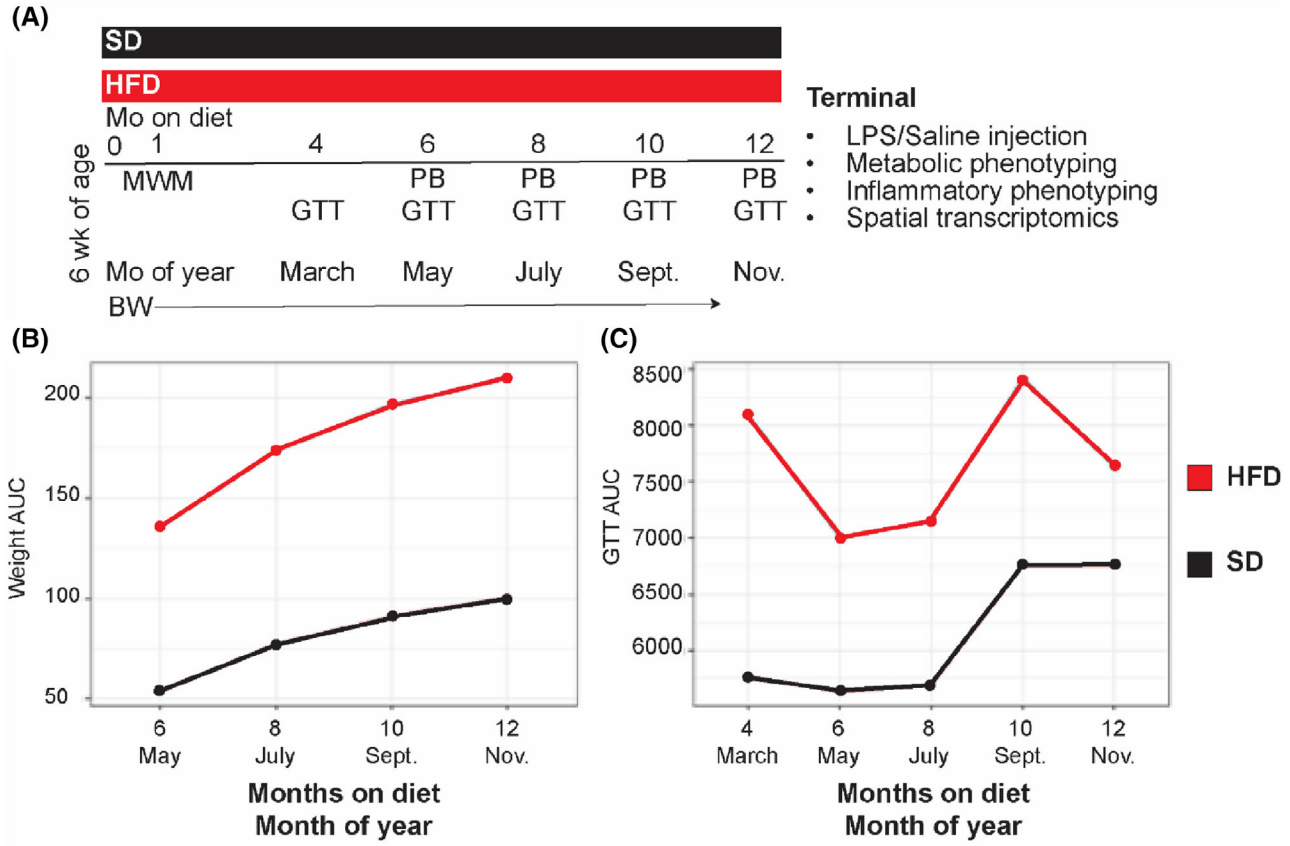

(D)

WEIGHT AUC CONTRAST	MO ON DIET MO OF YR	SD	HFD	DIFFERENCE	95% LB	95% UB	*P*-VALUE
SD/HFD	6 (MAY)	53.80	135.61	-81.80	-87.18	-76.43	1.39E-113
SD/HFD	8 (July)	77.07	173.57	-96.50	-101.41	-91.60	1.54E-152
SD/HFD	10 (Sept.)	91.01	196.82	-105.81	-112.75	-98.87	7.55E-114
SD/HFD	12 (Nov.)	100.57	209.84	-109.28	-116.22	-102.34	2.03E-118

(E)

GTT AUC CONTRAST	MO ON DIET MO OF YR	SD	HFD	DIFFERENCE	95% LB	95% UB	*P*-VALUE
SD/HFD	4 (March)	5766.3	8092.7	-2326.4	-3113.58	-1539.22	3.47E-08
SD/HFD	6 (May)	5644.9	7005.4	-1360.5	-2147.68	-573.32	8.30E-04
SD/HFD	8 (July)	5691.8	7152.1	-1460.3	-2247.48	-673.12	3.47E-04
SD/HFD	10 (Sept.)	6758.3	8416.2	-1657.9	-2445.08	-870.72	5.45E-05
SD/HFD	12 (Nov.)	6761.9	7633.5	-871.575	-1672.69	-70.46	0.033198

FIGURE 1 Study design and longitudinal metabolic phenotyping. Data from $n = 15$ SD and $n = 15$ HFD mice over 1 year of feeding. A, Study design. B, Body weight AUC (see Figure S1 in supporting information for details on body weight AUC calculation). C, GTT AUC. D, Difference between groups in body weight AUC. E, Difference between groups in GTT AUC. A Cox proportional hazards model was used to compare differences in AUC between groups. AUC, area under the curve; BW, body weight; GTT, glucose tolerance test; HFD, high-fat diet; LB, lower bound; LPS, lipopolysaccharide; MO, month; MWM, Morris water maze; Nov., November; PB, puzzle box; SD, standard diet; Sept., September; UB, upper bound; wk, weeks; YR, year.

In the CNS, we quantified hippocampal microglial morphology as a surrogate of microglial activation (Figure 3A; Figures S9 and S10). We found that microglia of saline-treated HFD mice had fewer branch points in the hilus region versus saline-treated SD mice (Figure S10B). Upon LPS stimulation, HFD microglia had little to no change in multiple morphological characteristics, whereas SD microglia responded as expected, becoming more ameboid with smaller territorial and cell volumes, lower complexity (i.e. ramification), and fewer end and branch points (Figure 3; Figures S9 and S10). This was particularly evident in cellular complexity, which decreased significantly in LPS-stimulated SD microglia in the hilus and molecular layer regions (Figure 3B). Conversely, there was no change in cellular complexity of HFD microglia in

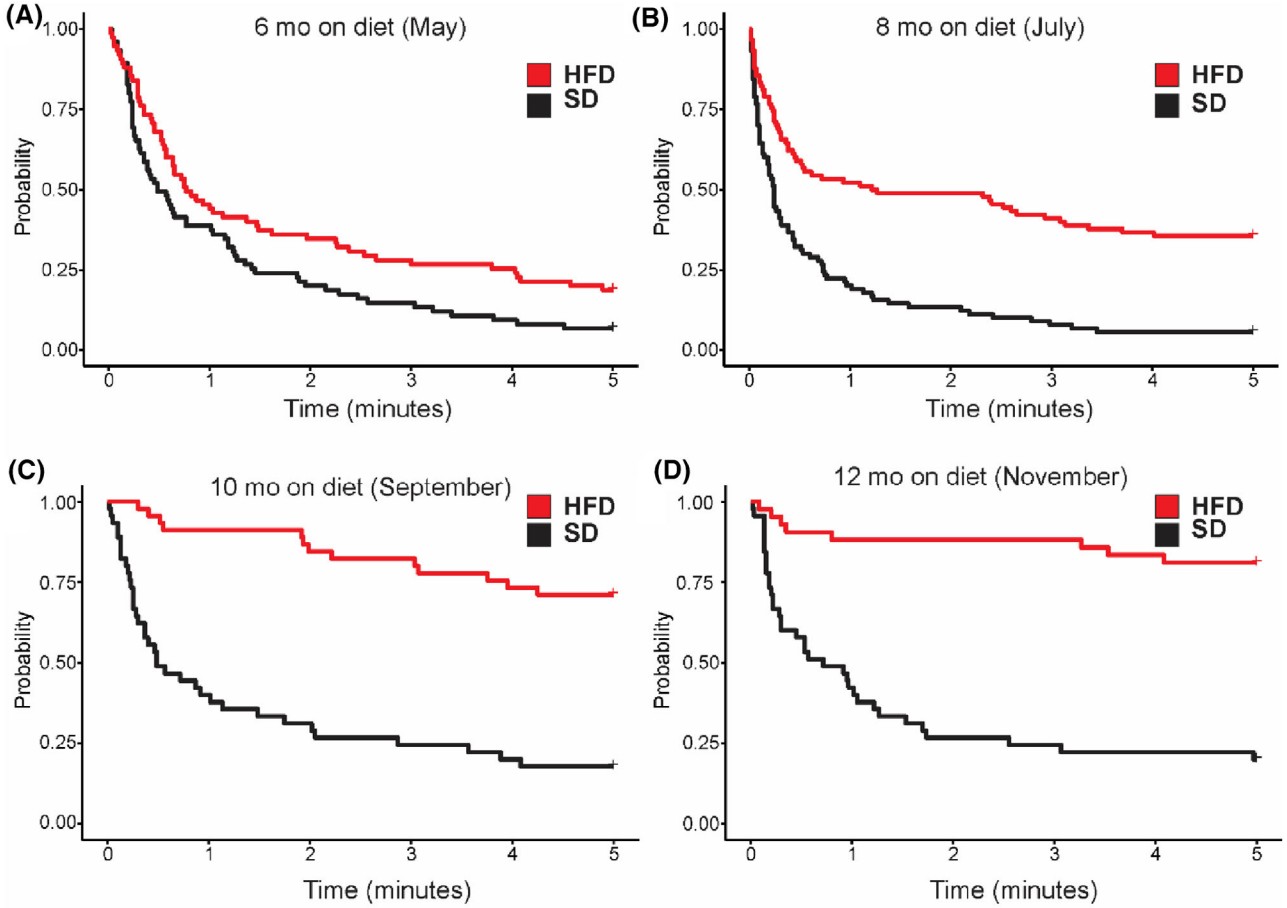

FIGURE 2 Kaplan–Meier curves for longitudinal puzzle box data. Data from $n = 15$ standard diet (SD) and $n = 15$ high-fat diet (HFD) mice after (A) 6 months (May); (B) 8 months (July); (C) 10 months (September); (D) 12 months on diet (November). Kaplan–Meier survival probability was calculated and represents the average probability of each group to escape the light area of the box to the dark area. A longer escape time is the adverse event associated with poorer task performance.

response to LPS, indicating a significantly impaired ability to respond to inflammatory stimuli.

3.4 | Chronic HFD alters brain spatial transcriptomic profiles

Our murine data show persistent metabolic stress and CI due to HFD, coupled with terminal inflammatory changes, including hippocampal microglial morphology. To further identify potential underlying mechanisms of these effects, we analyzed differences in brain spatial transcriptomics. We identified 24 unique gene expression clusters (Figure S11 in supporting information) localized to distinct brain regions, including hippocampal regions (Figure S11A). To generate biological insight, we performed gene set variation analysis (GSVA; Table S2 in supporting information), identified DEGs (Table S3 in supporting information), conducted DEG pathway enrichment using KEGG (Table S4 in supporting information), and assessed cell–cell communication using ligand receptor pairs via CellChat.

Overall, HFD caused changes in cluster representation (i.e., changes in percentage; Figure S11C), indicating spatially distinct changes in gene expression due to diet. HFD also enriched neurodegenerative and inflammatory or immune response pathways across bioinformatic analyses, indicating that these biological pathways were strongly impacted by diet. For example, we found enrichment of complement and coagulation cascades with GSVA analysis (Figure S12 in supporting information; Table S2) and Fc gamma R-mediated phagocytosis with KEGG analysis (Figure S13 in supporting information; Table S4). To understand changes in signaling between clusters using CellChat analysis (Figure S14 in supporting information), we found that HFD decreased the number of cluster interactions, but increased their strength (Figure S14A,B). LPS decreased the number and strength of interactions in SD mice, but in HFD mice increased the number of interactions while decreasing interaction strength (Figure S14A,B). HFD also altered the signaling pathways related to these changes (Figure S14C,D), indicating that HFD causes significant and spatially distinct shits in communication in the brain. Specific signaling pathways altered by HFD included increased signaling related to amyloid precursor protein (APP) and SPP1, a pro-inflammatory factor that upregulates IFN-γ and interleukin 12 (IL-12) expression (red text in Figure S14C). In LPS animals, HFD also upregulated inflammatory signaling pathways, such as activin (pink text in Figure S14D). Together, these changes

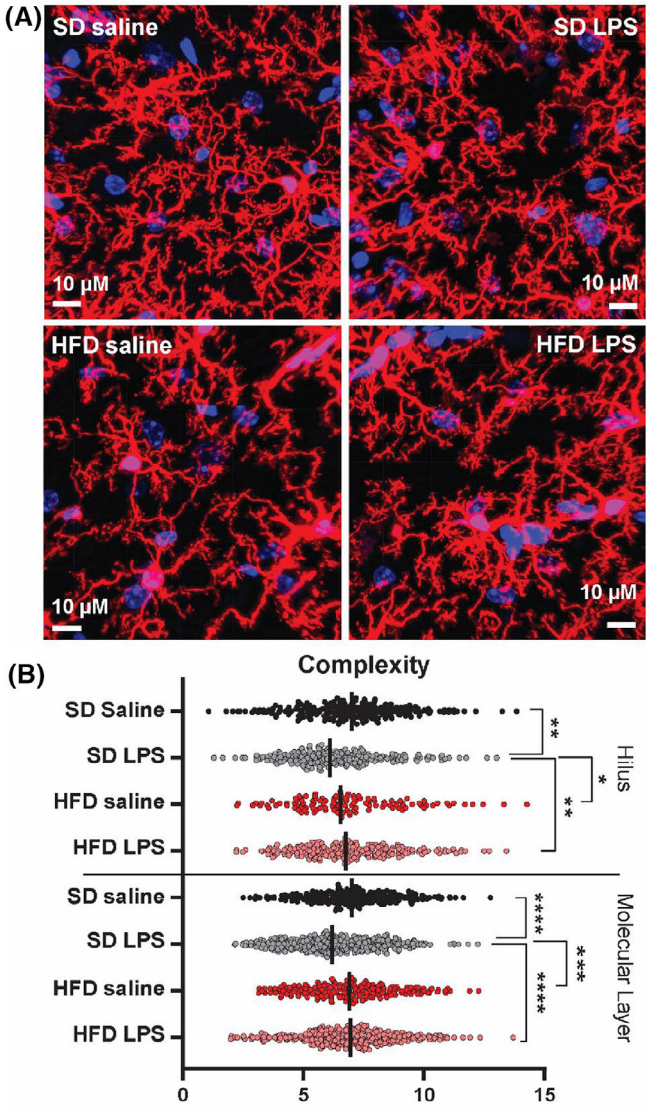

FIGURE 3 Terminal hippocampal microglial morphology. Data from $n = 13$ SD ($n = 6$ saline, $n = 7$ LPS) and $n = 11$ HFD ($n = 4$ saline, $n = 7$ given LPS) mice after 1 year of feeding. Terminal hippocampal microglial morphology with (A) representative images from all four groups; (B) complexity score for hilus (top) and molecular layer (bottom) microglia. Data are presented individual data points (cells) with means (black bars) and analyzed using mixed model. Differences are annotated as $^{*}P < 0.05$, $^{**}P < 0.01$, $^{***}P < 0.001$, $^{****}P < 0.0001$. There were no significant differences in complexity in the CA1 region (data not shown). HFD, high-fat diet; LPS, lipopolysaccharide; SD, standard diet.

indicate that many of the transcriptomic changes due to HFD in the brain are spatially distinct, involve neurodegenerative or inflammatory pathways, and that communication related to these pathways is also impacted due to diet.

To narrow our results and focus on the clusters with the most significant changes due to HFD, we first focused on clusters with a large change in representation due to HFD and found that many of these clusters had a high proportion of glial cells (Figure S15 in supporting information). Next, we selected clusters with a unique gene expression profile due to diet. Finally, we selected clusters based on location (brain region). In these selected clusters of interest (clusters C0, C7, C11, and C15), KEGG pathway analysis showed that HFD-enriched pathways related to many neurodegenerative pathways or diseases, such as AD and Huntington's disease, in both saline- (Figure 4A) and LPS-treated (Figure S16 in supporting information) mice (Table S4). Metabolic pathways, such as T2D, were also enriched, along with inflammatory or immune-related pathways, including inflammatory mediator regulation of transient receptor potential (TRP) channels (Figure 4A). These enrichment results indicate that, as in our overall analysis, many of the HFD-induced transcriptomic changes involve neurodegenerative, metabolic, and inflammatory pathways, highlighting their importance in disease. Using DEGs within these pathways to further identify specific targets of interest, we identified an upregulation of complement C1q A chain (C1qa), a critical complement component protein,[43] and nuclear factor kappa light chain enhancer of activated B-cells inhibitor alpha (*NFκBIA*), a regulator of the pro-inflammatory transcription factor NFκB (Table S3)[44,45] in HFD mice. Using CellChat analysis to identify shifts in communication between these clusters of interest due to diet (Figure 4B,C, saline mice; Figure S16, LPS mice), we also found both increased and decreased communication, dependent upon cluster and treatment (i.e., saline vs. LPS). Interestingly, HFD altered SPP1 and V-type immunoglobulin domain-containing suppressor of T-cell activation (VISTA) signaling in saline mice (Figure 4B,C) and semaphorin (SEMA) signaling in LPS mice (Figure S16B,C). These results further indicate dysregulated brain inflammatory and immune signaling due to HFD, with a particular emphasis on innate immune mechanism such as SPP1 signaling.

3.5 | Human subjects

To translate our murine findings and increase their human relevance, we obtained six *post mortem* human hippocampal samples. Of these human subjects (subject information in Table S5 in supporting information), three were controls and three were diagnosed with T2D and AD (AD+T2D). Two samples (one control and one AD+T2D, denoted by asterisks in Table S5) were selected for spatial transcriptomics. All samples were submitted for scRNA-seq to validate spatial transcriptomics data.

3.6 | AD subjects with T2D have altered hippocampal spatial transcriptomic profiles

In our human dataset, we identified 17 unique, spatially distinct gene expression clusters by spatial transcriptomics (Figure S17 in supporting information). To generate biological relevance, we performed similar analyses as in our murine dataset: GSVA (Table S6 in supporting information), DEG identification (Table S7 in supporting information), KEGG pathway enrichment (Table S8 in supporting information), and CellChat. Overall, AD+T2D caused changes in cluster representation for most clusters (Figure S17), and we consistently found changes in

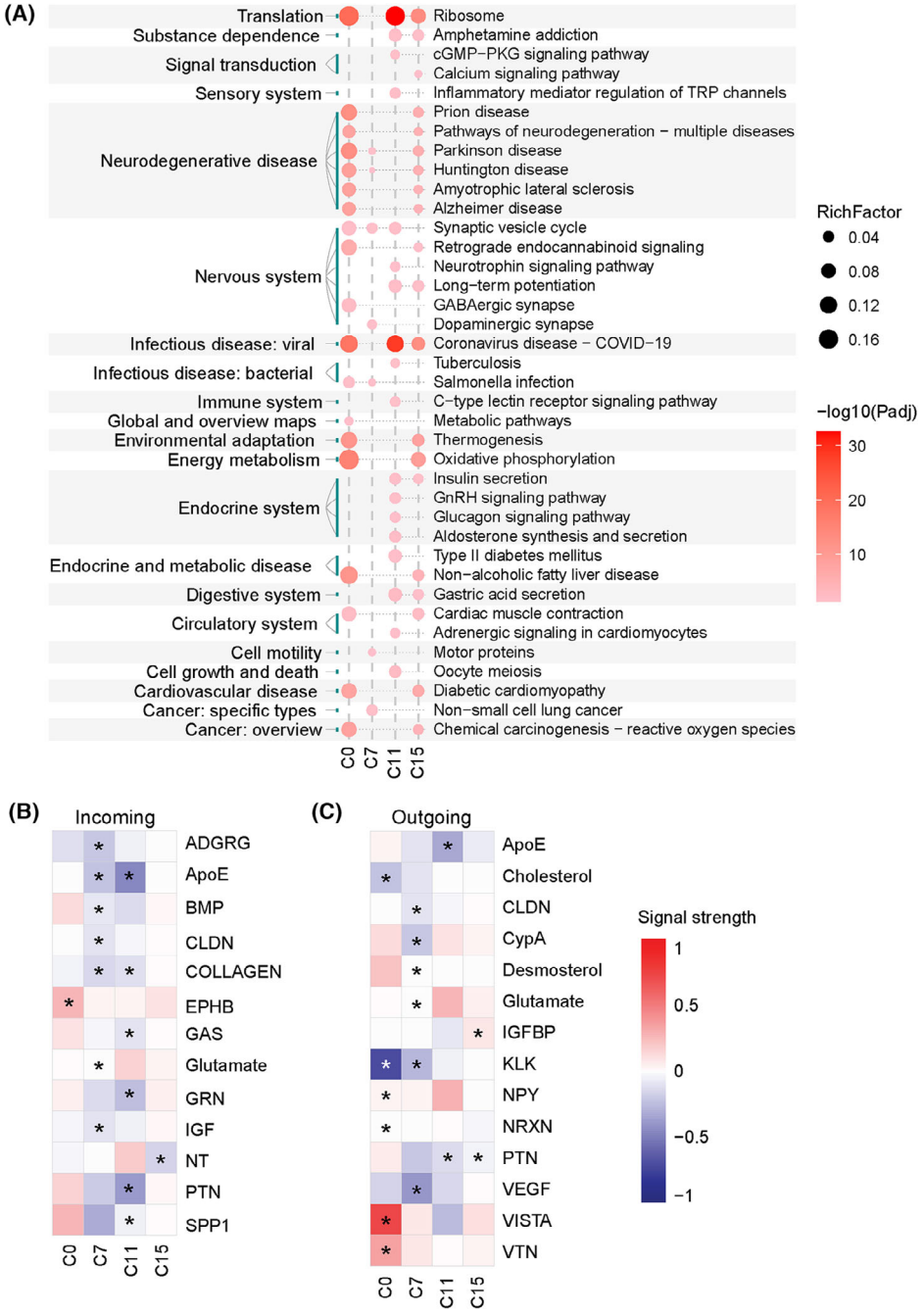

FIGURE 4 Mouse brain spatial transcriptomics enrichment analysis. Data from the clusters of interest (C0, C7, C11, C15) from standard diet (SD; $n = 3$ biological and $n = 1$ technical replicates) and high-fat diet (HFD; $n = 3$ biological and $n = 1$ technical replicates) mice given saline after 1 year of feeding. A, Kyoto Encyclopedia of Genes and Genomes (KEGG) pathway analysis. Rich factor represents the ratio of significant differentially expressed genes within a pathway to the total number of genes and is denoted by dot size. Dot color indicates significance from less (pink) to most (red) significant on a log10 adjusted *P* value scale. CellChat incoming (B) and outgoing (C) signaling pathways based on the CellChat database, in which signaling pathways are composed of ligand–receptor complexes. Asterisks represent significant ($P < 0.05$) differences in signaling pathways due to HFD. Heatmaps indicate the strength of the incoming or outgoing signal from one cluster to another with a deeper red representing a greater upregulation of signal activity and a deeper blue indicating a greater downregulation of signal activity.

neurodegenerative pathways and enrichment of multiple inflammatory or immune response pathways with all bioinformatic analyses. This indicates that, as in the murine data, AD+T2D causes gene expression changes specific to brain region, and that many of these changes are related to biological pathways involving neurodegeneration and the immune response. For example, there was significant enrichment of antigen processing and presentation using GSVA analysis (Figure S18 in supporting information; Table S6) and cellular senescence using KEGG analysis (Figure S19 in supporting information; Table S8). CellChat showed that AD+T2D increased both the number and

strength of cell–cell interactions (Figure S20A,B in supporting information). AD+T2D also significantly altered associated biological signaling pathways (Figure S20C), including increased APP and SPP1 signaling. This points to not only overall transcriptomic changes due to disease but also changes in brain communication similar to those observed in our murine dataset.

Cluster cell type composition (Figure S21A in supporting information) indicated that many of the clusters had a high proportion of glial cells. Shifts in cell populations due to AD+T2D included an increase in microglia (Figure S21B) and changes in neuronal populations (particularly a decrease in neuron 1; Figure S21C). Therefore, to narrow our results and focus on clusters most impacted by disease, we identified C3, C4, C5, C7, and C13 as clusters of interest based on a large change in cluster representation or in AD normalized enrichment score (with GSVA) due to AD+T2D, a high proportion of glial cells, and a unique gene expression profile. In our clusters of interest, KEGG analysis showed enrichment of many neurodegenerative pathways, including AD (Figure 5; Table S8). Metabolic pathways, such as insulin signaling pathway and insulin secretion, were also enriched, along with inflammatory or immune related pathways, including leukocyte transendothelial migration and complement and coagulation cascades (Figure 5A). These data indicate that in our clusters of interest which have a high concentration of glial cells, similar to our murine data and our overall human results, AD+T2D shifts transcriptomic profiles to promote a neurodegenerative and neuroinflammatory milieu in the brain. DEGs within significant pathways further identified targets of interest, and included upregulation of C1QA, and NFκBIA (Table S7), which were also upregulated in our murine analysis. CellChat also identified shifts in cell–cell communication due to AD+T2D (Figure 5B,C), including increased APP communication (incoming and outgoing). We similarly found changes (primarily increases) due to AD+T2D in inflammatory signaling. These included increased SPP1 and SEMA signaling (Figure 5B,C), supporting our hypothesis that inflammation and immune system dysregulation play a pivotal role in CI. Together our data show alignment between murine and human spatial transcriptomics results, indicate a strong role for neurodegenerative and inflammatory mechanisms, confirm that glia contribute to disease, and identify potential inflammatory mediators or signaling, namely SPP1 and SEMA.

3.7 | Conserved brain spatial transcriptomic profiles between mice and humans

To further narrow our analysis to identify specific mechanistic targets of interest along the continuum of metabolic stress and with CI, we compared transcriptomic profiles significantly altered due to diet in saline-treated mice or AD+T2D in humans. We found ≈ 44% (171 of 388) of mouse DEGs and ≈ 79% (30 of 38) of mouse KEGG pathways overlapped with humans (Table S9 in supporting information). Many of these common genes and pathways were related to neurodegenerative diseases or the nervous system, such as AD or long-term potentiation. We also observed a common enrichment of metabolic and inflammatory pathways, including energy metabolism and inflammatory mediator regulation of TRP channels.

In CellChat analysis, we found seven overlapping signaling pathways: APP, collagen, glutamate, L1 cell adhesion molecule (L1CAM), neurotrophin (NT), SEMA4, and SPP1 (Figure 6). Of these, we focused on APP for its classic role in AD (Figure 6A-D) and SPP1 for its role in inflammation (Figure 6E-H). APP signaling was significantly upregulated between most clusters in both AD+T2D and HFD (Figure 6A,B). While there were no major differences in APP-related ligand–receptor pairs due to AD+T2D or HFD, there were differences between species. In humans, APP-CD74 and APP-SORL1 (sortilin related receptor 1) were the major contributors, whereas App-Sorl1 and App-Tnfrsf21 (tumor necrosis factor receptor superfamily member 21) were the major contributors in mice (Figure S22 in supporting information). In humans, SPP1 signaling was strongly upregulated due to AD+T2D in almost all clusters. A similar but less robust pattern was observed in murine clusters due to HFD (Figure 6E,F). Interestingly, cluster 0, a murine cluster of interest with a high proportion of microglia, was the primary cluster from which increased SPP1 signaling originated. Like APP ligand–receptor interactions, major differences were noted only between species, not due to HFD or AD+T2D. In humans, *SPP1–CD44* interaction had the strongest influence on SPP1 signaling. Conversely, in mice *SPP1-ITGA+ITGAB* (integrin receptor alpha + integrin receptor beta) was the biggest contributor (Figure S22). Therefore, although we found unique changes across species, our murine data closely mirror data from humans and strongly support a role for SPP1 signaling in disease.

3.8 | Brain spatial transcriptomic validation

To validate our human spatial transcriptomics data, we used scRNA-seq data from all six human subjects. As in the spatial data, AD+T2D decreased the percentage of neurons and increased the percentage of microglia (Figure S23 in supporting information). Neurons and microglia also had the largest number of DEGs due to AD+T2D (Table S10 in supporting information), indicating that these cell types were the most impacted by disease in our dataset. Significantly enriched pathways due to AD+T2D in microglia included many inflammatory pathways, such as complement and coagulation cascades and B cell receptor signaling pathway (Figure S24; Table S11 in supporting information). This supports our spatial data showing a strong role for inflammation in disease. Within neurons, significantly enriched pathways included neurodegenerative pathways, such as AD, and inflammatory or metabolic pathways, such as inflammatory mediator regulation of TRP channels (Table S11). These data also support a role for inflammation in AD+T2D, even in non–immune cell types such as neurons. We similarly confirmed our targets of interest from our spatial analysis using DEGs, specifically *APP*, *SPP1*, *C1QA*, and *SEMA4*. Together, these data support our spatial transcriptomics results and further demonstrate a role for microglia and inflammation in AD+T2D.

We also performed qPCR for App, Sema4, and Spp1 in murine hippocampal tissue (Figure S25 in supporting information) and IHC with

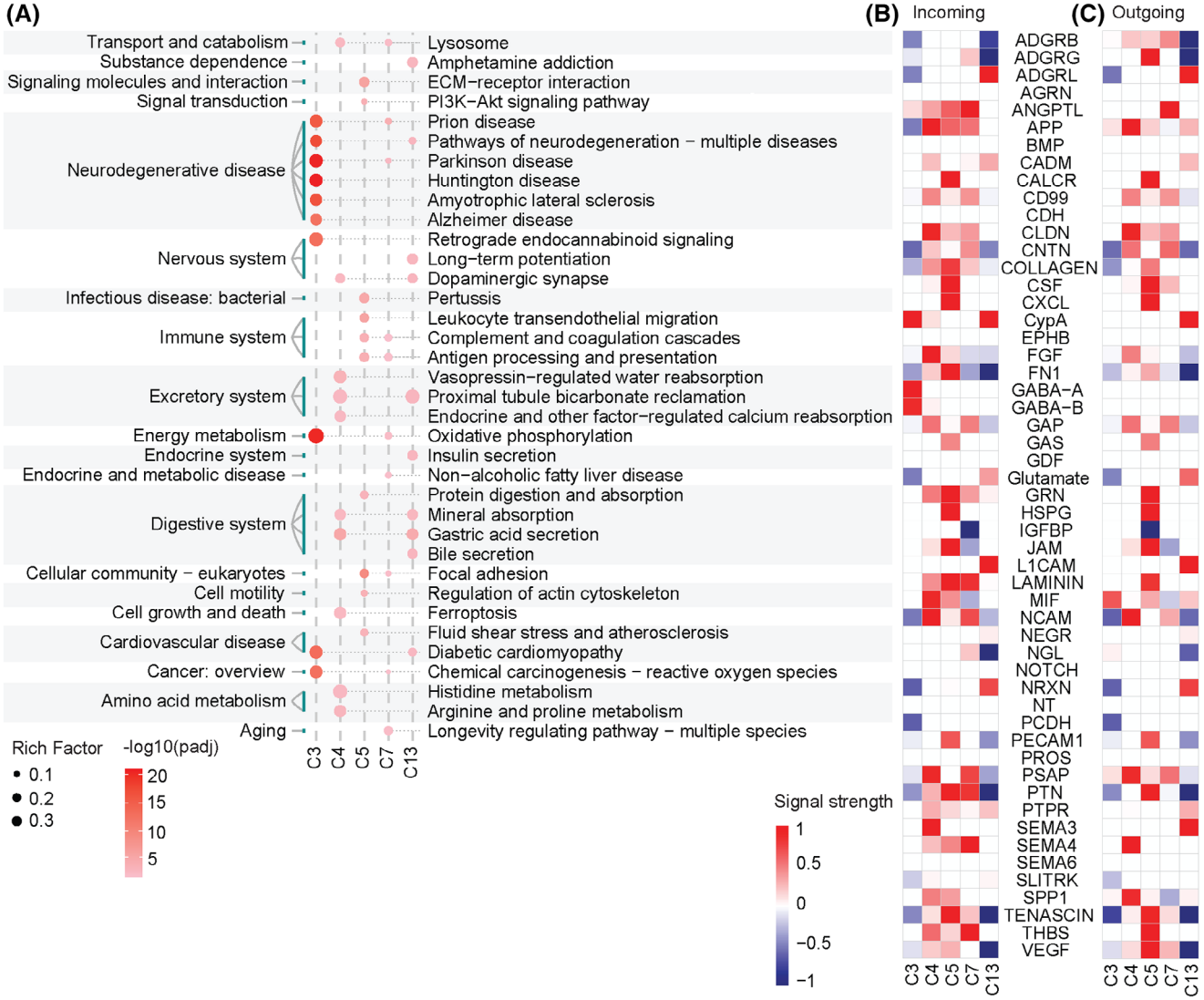

FIGURE 5 Human spatial transcriptomics enrichment results. Data from the hippocampal clusters of interest (C3, C4, C5, C7, C13) from control ($n = 1$) and Alzheimer's disease and type 2 diabetes ($n = 1$) patients. A, Kyoto Encyclopedia of Genes and Genomes (KEGG) pathway analysis. Rich factor represents the ratio of significant differentially expressed genes within a pathway to the total number of genes and is denoted by dot size. Dot color indicates significance from less (pink) to most (red) significant on a log10 adjusted *P* value scale. CellChat incoming (B) and outgoing (C) signaling pathways based on the CellChat database, in which signaling pathways are composed of ligand–receptor complexes. Heatmaps indicate the strength of the incoming or outgoing signal from one cluster to another with a deeper red representing a greater upregulation of signal activity and a deeper blue indicating a greater downregulation of signal activity.

subsequent RNAscope for SPP1 and C1qa expression in hippocampal microglia to validate our targets of interest. In saline mice, *APP* gene expression was higher in HFD versus SD mice. Furthermore, HFD animals had a significant decrease in *APP* in response to LPS, whereas SD animals had no change (Figure S25A). There was a similar pattern for *SEMA4* gene expression, in which pairwise comparisons showed a trending increase in *SEMA4* in HFD versus SD saline animals and a significant decrease in HFD mice due to LPS treatment (Figure S25B). For *SPP1*, LPS administration had no effect, but there was a trending overall effect of diet, with higher *SPP1* gene expression due to HFD (Figure S25C). Similarly, RNAscope showed a strong trend for an increase in SPP1 in microglia in the CA1 ($P = 0.0553$) and molecular layers ($P = 0.0537$) of the hippocampus, and a numeric but non-significant increase in *C1qa* gene expression in all three hippocampal regions measured (Figure S25D-J).

Given the potential role of SPP1, particularly in microglia, we next performed in vitro experiments in a human microglial cell line. We incubated these cells with the saturated fatty acid palmitate to mimic an obesogenic environment and assessed inflammatory responses and cell death (Figure S26 in supporting information). We found that obesogenic conditions induced an inflammatory environment, increasing the production of the pro-inflammatory cytokines TNF-α and MMP-9 (Figure S26A,B). In addition, obesogenic conditions increased cell death, as measured by increased caspase activity (Figure S26I).

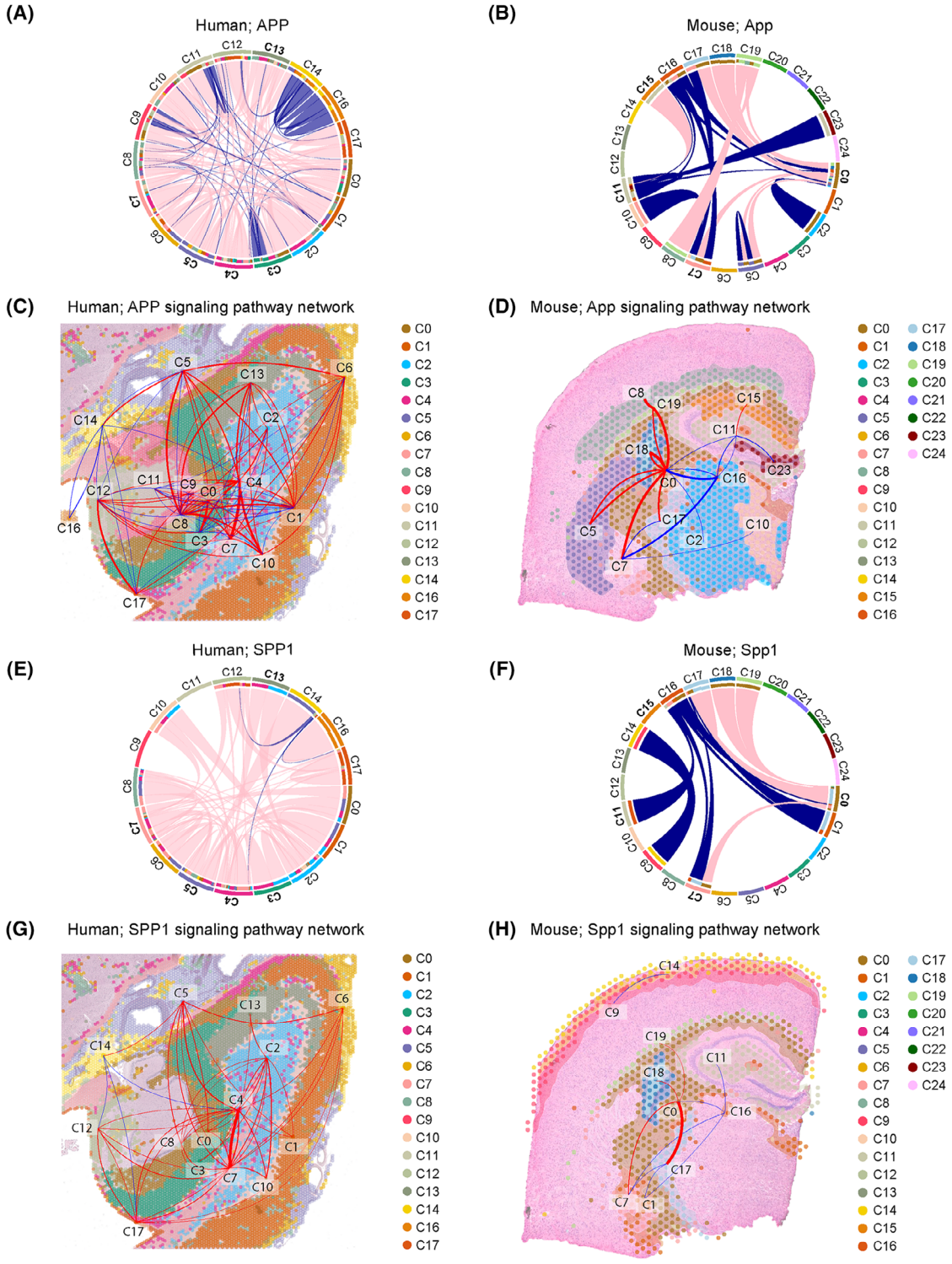

FIGURE 6 Overlapping cell–cell signaling pathways between murine and human spatial transcriptomics data. Murine data from standard diet (SD; $n = 3$ biological and $n = 1$ technical replicates) and high-fat diet (HFD; $n = 3$ biological and $n = 1$ technical replicates) mice given saline and human data from a control (Ctrl) patient ($n = 1$) and a patient with Alzheimer's disease and type 2 diabetes (AD+T2D; n = 1). Amyloid precursor protein (APP) circle plots in humans (A) and mice (B). Autocrine and paracrine signaling interactions between clusters are represented with color indicating upregulated (red) or downregulated (blue) interactions in AD+T2D or with HFD. Bolded clusters indicate clusters of interest. Mapped APP in humans (C) and mice (D). Signaling interactions between clusters are represented with colors indicating upregulated (red) or downregulated (blue) interactions in AD+T2D or with HFD. Secreted phosphoprotein 1 (SPP1) circle plots in humans (E) and mice (F). Autocrine and paracrine signaling interactions between clusters are represented with colors indicating upregulated (red) or downregulated (blue) interactions in AD+T2D or with HFD. Mapped SPP1 in humans (G), and mice (H). Signaling interactions between clusters are represented with colors indicating upregulated (red) or downregulated (blue) interactions in AD+T2D or with HFD. Wilcoxon rank testing was performed to compare HFD and SD in mice, and only the significant interactions are displayed in the figures.

(A) Group	Female	Male	Black or African American	White	Age range (yrs)	Avg PMI +/- SD (hrs)	2+ regions	3 brain regions
Ctrl (n=36)	67%	33%	44%	56%	64-89; n=10 >90	13+/-12	78%	42%
AD (n=87)	66%	34%	31%	68%	68-89; n=53 >90	10+/-6	85%	60%
n=1 AD patient was classified as an American Indian or Alaska Native								

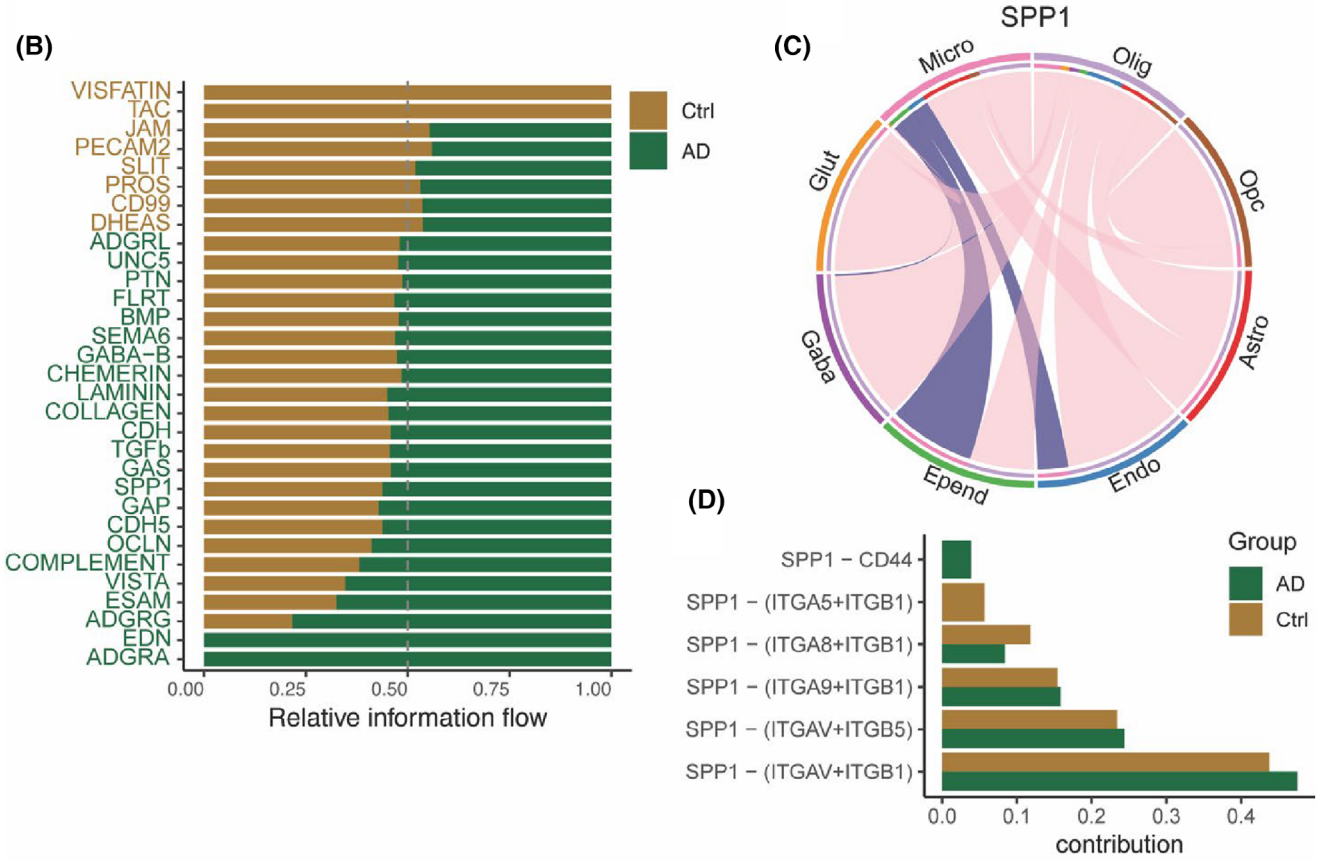

(E) Cell-signaling pathway	Human spatial	Human/mouse
SPP1		
COLLAGEN		
GAS		x
LAMININ		x
BMP		x

FIGURE 7 AMP-AD participant demographics, *post mortem* brain single-nucleus RNAseq CellChat analysis (based on ligand–receptor pairs), and overlapping signaling pathways between datasets. Data are presented as (A) demographics, (B) significantly altered cell–cell signaling pathways, (C) SPP1 signaling circle plot, (D) contributing ligand–receptor pairs to SPP1 signaling, and (E) overlapping significant CellChat signaling pathways in spatial transcriptomics and AMP-AD data. If a single participant had data from multiple brain regions (caudate nucleus, superior temporal gyrus, and dorsolateral prefrontal cortex), data were pooled. In the circle plot, autocrine and paracrine signaling interactions between cell types are represented with color indicating upregulated (red) or downregulated (blue) interactions in AD. Overlapping pathways (red shaded cells) indicate signaling pathways shared between AMP-AD data and human spatial transcriptomics data and/or the human/mouse spatial transcriptomic crossover analysis. AD, Alzheimer's disease; AMP-AD, Accelerating Medicines Partnership–Alzheimer's Disease; Ctrl, control; PMI, *post mortem* interval; SD, standard deviation; SPP1, secreted phosphoprotein 1.

3.9 | Human brain transcriptomics validation

To further validate our analyses, and to increase translational relevance to the larger population, we compared our human and murine datasets to a larger and more diverse brain single nucleus RNAseq database obtained through the AD Knowledge portal, specifically the AMP-AD dataset. Within these data, control ($n = 36$) and AD participants ($n = 87$; participant demographics in Figure 7A) were selected; however, data related to obesity or diabetes status was not available and thus not included.

Control and AD participants had a similar cell-type distribution of the major cell types identified (Figure S27 in supporting information).

	Avg Rank	App	Sorl1	Tyrobp	Cd74	Spp1	Itgav	Itgb1	Itgb5	Itga8	Itga5	Avg. Cplx. Hilus	Avg. Cplx. Mol. Layer	%cells Q1 Hilus	%cells Q4 Hilus	%cells Q1 Mol. Layer	%cells Q4 Mol. Layer
Avg Rank		0.56			-0.52	0.56						**-0.93**	*-0.75*	*0.84*	*-0.81*	*0.78*	*-0.81*
App	0.56		-0.65			0.70	0.64					-0.53	**-0.87**	0.52	*-0.83*	**0.90**	-0.71
Sorl1		-0.65						0.54	0.52	*0.81*		0.65	0.55			-0.57	
Tyrobp					0.51			0.50		0.62					0.62		
Cd74	-0.52			0.51								0.71	*0.74*	-0.76	**0.90**	-0.52	**0.83**
Spp1	0.56	0.70					**0.85**						-0.72	*0.83*		**0.89**	-0.54
Itgav		0.64				**0.85**		*0.76*		0.55	0.55		-0.62			*0.73*	
Itgb1			0.54	0.50			*0.76*		**0.83**	**0.89**	**0.90**	0.63					
Itgb5			0.52					**0.83**		0.69	**0.92**	0.78		-0.72			
Itga8			*0.81*	0.62			0.55	**0.89**	0.69		*0.75*	0.64					
Itga5							0.55	**0.90**	**0.92**	*0.75*		*0.82*		-0.56			
Avg. Cplx. Hilus	**-0.93**	-0.53	0.65		0.71			0.63	0.78	0.64	*0.82*		0.71	*-0.82*	*0.81*	-0.73	0.78
Avg. Cplx. Mol. Layer	*-0.75*	**-0.87**	0.55		*0.74*	-0.72	-0.62					0.71		-0.72	**0.92**	**-0.93**	**0.95**
% cells Q1-Hilus	*0.84*	0.52			-0.76	*0.83*			-0.72		-0.56	*-0.82*	-0.72		-0.61	*0.88*	-0.69
% cells Q4-Hilus	*-0.81*	*-0.83*		0.62	**0.90**							*0.81*	**0.92**	-0.61		*-0.81*	**0.98**
% cells Q1-Mol. Layer	*0.78*	**0.90**	-0.57		-0.52	**0.89**	*0.73*					-0.73	**-0.93**	*0.88*	*-0.81*		*-0.80*
% cells Q4-Mol. Layer	*-0.81*	-0.71			**0.83**	-0.54						0.78	**0.95**	-0.69	**0.98**	*-0.80*	

FIGURE 8 Heat map representing the correlative analysis among murine behavior, gene expression, and microglial morphology. Analysis measured the correlations between behavior (as average rank), gene expression data for *APP* (*APP*, *SORL1*, *TYROBP*, and *CD74*) and *SPP1* (*SPP1*, *ITGAV*, *ITGB1*, *ITGB5*, *ITGA8*, and *ITGA5*) related signaling, and microglial morphology. Color represents the correlation strength (darker red = stronger positive correlation, darker blue = stronger negative correlation), with strong correlations (Pearson correlation coefficient; PCC > 0.5) included on the heat map. Data analyzed Pearson correlation analysis and significant PCC ($P < 0.05$) are indicated in bold and trending PCC in italics ($P < 0.1$). For quartiles, cellular complexity data were divided into four quartiles and the percentage of cells that fell within the two outermost quartiles of complexity (Q1 and Q4) were included in the analysis. A greater percentage of cells within Q1 is indicative of a high degree of activation, whereas a greater percentage of cells within Q4 is indicative of a low degree of activation (quartile 4). Avg, average; Cplx, complexity; Mol, molecular; Q, quartile.

DEG (Table S12 in supporting information) and KEGG analysis showed alteration in multiple genes and pathways (Table S13; Figure S28 in supporting information) related to neurodegeneration and immune pathways or inflammation, such as complement and coagulation cascade, similar to our spatial transcriptomics data. Indeed, 69% of our significantly enriched KEGG pathways due to AD+T2D overlapped with significant AMP-AD KEGG pathways due to AD.

CellChat analysis also indicated a good agreement between the larger and more diverse AMP-AD data and our spatial transcriptomics data. Overall, we found a mild increase in signaling strength due to AD, with neurons (gabaergic and glutamatergic) and oligodendrocyte precursor cells as the biggest contributors to increased signaling in both control and AD participants (Figure S29 in supporting information). CellChat analysis also identified significantly altered signaling pathways similar to those observed in our spatial transcriptomics and human mouse cross-over analysis (Figure 7B-E). Importantly, we identified a significant increase in SPP1 signaling due to AD, which was consistent among all three datasets. In total, we were able to validate our translationally relevant genes of interest in mouse and human brain and show an increase in expression of hippocampal genes related to AD/ADRD and inflammatory pathways.

3.10 | Association among APP, SPP1, microglia, and cognition

Finally, to add additional physiological relevance to our data, we performed a correlative analysis using *APP* and *SPP1* signaling-related gene expression, microglial morphology, and cognitive outcomes (Figure 8). For our microglial data, we focused on cell complexity in the hilus and molecular layers as they were hippocampal regions with the greatest difference due to diet. We used both average microglial complexity and percentage of cells that fell within the two outermost quartiles, indicative of a high degree of activation (quartile 1) versus low degree of activation (quartile 4). For our behavioral data, we used the latency to escape from the terminal puzzle box to rank each animals' performance (average rank). Ranking placed the mouse with the shortest average time to escape first, that is, lower number/rank indicates better performance.

We found that poorer puzzle box performance correlated most highly with microglial activation. Further, there was an inverse correlation between behavior and microglial activation states, that is, greater percentage of activated microglia (quartile 1) was linked to poorer performance (positive correlation, indicated by a darker red color; Figure 8), whereas a greater percentage of resting microglia (quartile 4) was associated with better performance (negative correlation; indicated by a darker blue color; Figure 8). We also found a correlation between *APP* and *SPP1* signaling gene expression, behavior, and microglial morphology. For behavior, while not statistically significant, we found a strong correlation (Pearson correlation coefficient > 0.50) between both *APP* and *SPP1* and performance, in which a higher expression of both genes was associated with worse performance (i.e., higher rank). Multiple genes within *APP* and *SPP1* signaling pathways were significantly correlated with microglial morphology. For *APP*, *SPP1*, and *ITGAV*, a higher degree of microglial activation was correlated with increased gene expression. Additionally, a greater

percentage of activated microglia (quartile 1) correlated with increased gene expression, whereas a greater percentage of resting microglia (quartile 4) correlated with decreased gene expression. For *SORL1*, *CD74*, and *ITGA5*, this pattern was reversed, in which a higher degree of activation or the distribution of microglia in different activation states was associated with decreased gene expression. Together, these data indicate that these translationally relevant pathways and genes of interest are associated not only with microglial changes, but also with behavioral outcomes, showing their strong physiological relevance to disease.

4 | DISCUSSION

We found that HFD caused persistent metabolic and cognitive defects over 1 year of feeding. At the study end, mice exhibited inflammatory phenotypes, which were reflected in changes in brain spatial transcriptomic profiles. These included changes in cell–cell communication of inflammatory pathways, particularly between gene expression clusters with a high percentage of microglia. In AD+T2D human subjects, we observed similar changes in inflammatory pathways and signaling. Indeed, in our crossover analysis between mouse and human data, as well as in the larger and more diverse AMP-AD dataset, we found that many of the common pathways or signaling changes were related to inflammation, such as altered SPP1 signaling. We validated these findings and confirmed that AD- and inflammatory-related gene expression was elevated in brains and specifically in microglia from HFD animals. Further, we performed a correlative analysis to show that changes in gene expression, including increased *SPP1* and *APP* gene expression, along with a more activated hippocampal microglial morphology, were associated with worse murine behavioral outcomes. In total, our data support our hypothesis that microglial inflammatory mechanisms, including SPP1, contribute to CI and are common translationally relevant, pathologic factors.

We and others have previously shown that HFD causes obesity, metabolic dysfunction, and CI.[31,41,46–48] Here, we show that this metabolic and cognitive phenotype is progressive during chronic feeding. Furthermore, we show that metabolic factors, namely BW and glucose dysregulation, are predictive of future cognitive performance. Metabolic stressors typically progress along a continuum,[49] which is thought to promote CI due to shared disease-associated pathways, including those related to aging and inflammation.[50,51] Indeed, these shared pathways may represent early pathological events as data in humans indicate that metabolic factors, particularly midlife obesity, increase the risk for later life CI.[6,7]

In addition to the metabolic and cognitive dysfunction in our HFD animals, we also found peripheral and central inflammatory changes. Specifically, HFD mice had a blunted response to LPS in plasma TNF-α concentrations and in hippocampal microglial morphology. Previously, we noted that 3 days of HFD feeding did not alter plasma cytokine concentrations or response to LPS in 6-week-old mice.[24] However, we[31] and others[52–54] have reported that long-term HFD feeding increases plasma cytokine concentrations. Here, we also observed that SD mice remained responsive to LPS in their microglial morphology, but that HFD animals did not. This is consistent with our previous study in 6-week-old mice, where 3 days of HFD blunted response to LPS in terms of hippocampal microglia morphology.[24]

We observed few changes in morphology between saline-treated SD and HFD mice. There are reports that under unstimulated conditions, HFD alters microglial morphology to a state indicative of activation,[25–27] namely a more ameboid shape with fewer and shorter processes.[26,27] Here, limited differences between saline SD and HFD mice may be due to multiple factors. Microglial morphology is very plastic and can change rapidly in response to environmental cues,[55] or even tissue fixation protocols.[56] Importantly, aging alone can influence morphology,[57] and it is highly possible that age-related changes in our saline-treated mice overwhelmed diet-related differences. The chronic nature of this study (i.e., HFD feeding for 1 year) may have also triggered compensatory mechanisms in microglia, particularly in their unstimulated state. However, our HFD mice exhibited a loss of functionality in response to insult or injury, that is, LPS, supporting our contention that chronic HFD alters inflammatory profiles in the form of a reduced ability to respond to immune challenge.

A blunted response to LPS has been observed by others in *STAT3* activation in the brains of HFD fed rats.[58] Additionally, in aging[59] or metabolic stress,[59] cells (including microglia) can develop senescence, which is characterized by a loss of function and arrested cell cycle. Senescent cells also acquire a "senescence-associated secretory phenotype" with release of pro-inflammatory factors and cytokines, growth and death proteins, proteases, and extracellular matrix components.[60–62] Senescent microglia specifically can lose their ability to prune synapses and clear debris, such as protein aggregates like amyloid beta, which has been linked to CI.[63] We previously showed that changes in directionality of inflammatory gene expression due to HFD are dependent upon age: adult animals had an increase versus a decrease of the same inflammatory genes in middle-aged animals.[31] Therefore, an enrichment of inflammatory pathways in our transcriptomics results supports our data showing a reduced responsiveness to LPS, indicating a dysregulated immune or inflammatory milieu in the brain.

Indeed, our spatial transcriptomics analysis of murine brains showed a marked change in gene expression profiles due to HFD—specifically, altered neurodegenerative, metabolic, and inflammatory or immune pathways. These changes were primarily present in our clusters of interest, which contained a high percentage of glial cells. We also observed that HFD altered cell–cell communication, including signaling related to multiple inflammatory or immune response pathways. In parallel, spatial transcriptomics of human hippocampi show that AD+T2D resulted in similar changes with respect to gene expression cluster distribution and gene expression profiles. Neurodegenerative, metabolic, and inflammatory pathways and signaling were particularly prominent in AD+T2D clusters of interest, which had a high proportion of glial cells. Glial cells, particularly microglia, have long been implicated in neurodegenerative diseases, including AD/ADRD.[9,64,65] We and others have previously shown that microglia become aberrantly activated in mouse models of obesity and prediabetes,[24–27] as discussed above.

However, more studies are needed to fully understand inflammatory pathways that contribute to disease and the timeline of inflammatory events that contribute to progression in a cell-specific manner.

Analysis of common dysregulated genes or pathways across our murine and human datasets, including in the larger and more diverse AMP-AD dataset, further highlighted the importance of neurodegenerative, metabolic, and inflammatory or immune response pathways. Of these common inflammatory changes, disrupted SPP1 signaling emerged as a target of interest. Downstream SPP1 targets were identified as DEGs in mouse and human datasets, including *C1QA*, a critical component of the first step in the classic complement cascade,[43] and *NFκBIA*, a regulator of the pro-inflammatory transcription factor NFκB.[44,45] Similarly, we were able to validate increased SPP1 expression in murine hippocampal microglia and showed increased inflammatory responses and cell death under obesogenic conditions in a human microglial cell line. SPP1 was further validated as a common significantly altered signaling pathway in the AMP-AD dataset. Additionally, our correlative analysis showed that poorer cognitive outcomes in HFD mice were associated with a more activated hippocampal microglial morphology, and with higher *APP* and *SPP1* expression. *SPP1* encodes for the protein osteopontin (OPN), which is highly expressed in the CNS[66,67] and in microglia, particularly disease-associated microglia, and its expression increases with age.[68] Apart from its involvement in T_H1 immune responses and its actions as a chemokine/cytokine,[66,69] *SPP1*/OPN can promote type-1 interferon gene expression by activating interferon regulatory factor 7.[70] It can also associate with other proinflammatory signaling receptors or molecules to promote downstream pro-inflammatory responses.[71,72] Implicated in multiple neurodegenerative diseases, SPP1/OPN is increased in plasma and cerebrospinal fluid of AD/ADRD subjects and is linked to cognitive outcomes.[73] *SPP1* knockout can also reverse inappropriate microglial synaptic pruning in AD mouse models,[20] indicating an important role for this inflammatory pathway in disease pathology. Thus, SPP1 is a promising target of interest that should be interrogated for the treatment of metabolically driven CI.

While our studies implicate a role for microglial-mediated inflammation and inflammatory dysregulation in CI, it has some limitations. Our murine studies were only performed in male animals. It is widely recognized that there are differences due to sex in metabolic and inflammatory phenotypes and responses in both mice[74–76] and humans[74,77] and CI is more prevalent in females versus males. However, our analysis of AMP-AD data, which contains both male and female participants, shows good agreement with our spatial transcriptomics datasets. Further, studies are currently underway to better understand sexually dimorphic metabolic, inflammatory, and cognitive responses to HFD. We report changes in hippocampal gene expression and microglial morphology in HFD mice which associate with CI; however, we did not have access to cognitive assessments for our human subjects and cannot claim similar correlations here. Other studies support our contention that SPP1 has a role in regulating cognitive function, including an association between cortical *SPP1* gene expression and cognition in a large human cohort.[19] However, we did not determine the effects of cell type–specific *SPP1* knockout on cellular responses and cognitive outcomes in HFD mice. Similarly, we did not investigate pharmacological or other treatment options to block SPP1 signaling in vivo. These future experiments are the first step necessary to establish causality, confirm SPP1 as a therapeutic target, and take these findings into the clinic. While our transcriptomics data were performed on a limited number of samples, the agreement between our data and the larger existing AMP-AD dataset, along with the agreement between our murine and human data, we contend that our results support the hypothesis that inflammation and microglia are key drivers of CI and that SPP1 represents a viable mechanistic target for future research. Finally, while we have single-cell resolution in our human data, our murine data lacked this resolution. Subsequent studies are underway to elucidate the role of SPP1 and other inflammatory mechanisms in metabolically driven CI in a cell-specific manner.

Overall, we show that inflammation and immune-mediated mechanisms contribute to obesity and metabolically driven CI in mice and in humans. Further, we show that microglia play a critical role in mediating these mechanisms, with *SPP1* and the SPP1 pathway emerging as a key inflammatory pathway of interest in disease.

AUTHOR CONTRIBUTIONS

Conceptualization: Sarah E. Elzinga, Geoffrey G. Murphy, Eva L. Feldman. Methodology: Sarah E. Elzinga, Kai Guo, Ali Turfah, Rosemary E. Henn, Ian F. Webber-Davis, Crystal M. Pacut, Emily Glass, Adam M. Allouch, Dae-Gyu Jang, Rachel Parent, Kevin S. Chen, John M. Hayes. Investigation: Sarah E. Elzinga, Ali Turfah, Rosemary E. Henn, Ian F. Webber-Davis, John M. Hayes, Crystal M. Pacut, Andrew D. Carter, Diana M. Rigan, Adam M. Allouch, Dae-Gyu Jang, Emily Glass, Stephen I. Lentz. Visualization: Sarah E. Elzinga, Kai Guo, Ali Turfah, Kevin S. Chen. Funding acquisition: Sarah E. Elzinga, Eva L. Feldman. Project administration: Sarah E. Elzinga, Rosemary E. Henn, Diana M. Rigan. Supervision: Sarah E. Elzinga, Crystal M. Pacut, Diana M. Rigan, Rachel Parent, Geoffrey G. Murphy, Lili Zhao, Junguk Hur, Eva L. Feldman. Writing—original draft: Sarah E. Elzinga, Eva L. Feldman. Writing—review & editing: Sarah E. Elzinga, Kai Guo, Adam M. Allouch, Stephen I. Lentz, Geoffrey G. Murphy, Junguk Hur, Eva L. Feldman.

ACKNOWLEDGMENTS

Library prep and next-generation sequencing was carried out by the Advanced Genomics Core at the University of Michigan. Research reported in this publication was supported by the National Cancer Institutes of Health under Award Number P30CA046592 by the use of the following Cancer Center Shared Resource: Single Cell and Spatial Analysis Shared Resource. Human samples were obtained from the Michigan Brain Bank, a University of Michigan Alzheimer's Disease Core Center (P30AG053760/P30AG072931), a University of Michigan Alzheimer's Disease Core Center, and in collaboration with the Michigan Alzheimer's Disease Research Center. Authors would like to acknowledge Dr. Bhumsoo Kim for his technical assistance, Dr. Stacey Sakowski Jacoby for her assistance in applying for AD Knowledge Portal data, and Dr. Emily Koubek for her assistance in

formatting and submitting the manuscript. The results published here are in part based on data obtained from the AD Knowledge Portal (https://adknowledgeportal.org). Data generation was supported by the following NIH grants: P30AG10161, P30AG72975, R01AG15819, R01AG17917, R01AG036836, U01AG46152, U01AG61356, U01AG046139, P50 AG016574, R01 AG032990, U01AG046139, R01AG018023, U01AG006576, U01AG006786, R01AG025711, R01AG017216, R01AG003949, R01NS080820, U24NS072026, P30AG19610, U01AG046170, RF1AG057440, and U24AG061340, and the Cure PSP, Mayo and Michael J Fox foundations, Arizona Department of Health Services and the Arizona Biomedical Research Commission. The authors thank the participants of the Religious Order Study and Memory and Aging Project for the generous donation, the Sun Health Research Institute Brain and Body Donation Program, the Mayo Clinic Brain Bank, and the Mount Sinai/JJ Peters VA Medical Center NIH Brain and Tissue Repository. Data and analysis contributing investigators include Nilüfer Ertekin-Taner, Steven Younkin (Mayo Clinic, Jacksonville, FL), Todd Golde (University of Florida), Nathan Price (Institute for Systems Biology), David Bennett, Christopher Gaiteri (Rush University), Philip De Jager (Columbia University), Bin Zhang, Eric Schadt, Michelle Ehrlich, Vahram Haroutunian, Sam Gandy (Icahn School of Medicine at Mount Sinai), Koichi Iijima (National Center for Geriatrics and Gerontology, Japan), Scott Noggle (New York Stem Cell Foundation), Lara Mangravite (Sage Bionetworks). This work was supported by the National Institutes of Health (K99AG071667 to Sarah E. Elzinga, R01 DK130913 to Eva L. Feldman and Junguk Hur, P30EY007003 to Vision Research Center – SIL, P30DK020572 to Michigan Diabetes Research Center – SIL, P30AG053760/P30AG072931 to Michigan Brain Bank, University of Michigan Alzheimer's Disease Core Center, S10OD28612-01-A1 to SIL, P30CA046592 to Advanced Genomics Core); the Alzheimer's Association (AACSF-22-970586 to KSC); the Robert E. Nederlander Sr. Program for Alzheimer's Research (to Eva L. Feldman); the Andrea and Lawrence A. Wolfe Brain Health Initiative (to Eva L. Feldman); the Frank L. and Helen Gofrank Foundation Research Program in Alzheimer's Disease and Brain Health (to Eva L. Feldman); the Kiriluk Family Fund for Brain Health Research (to Eva L. Feldman); the Robert and Katherine Jacobs Environmental Health Initiative (to Eva L. Feldman); the Sinai Medical Staff Foundation Research on Studying Diet and Brain Health Fund (to Eva L. Feldman); the Kenneth and Frances Eisenberg Emerging Scholar Fund (to Kevin S. Chen); the Edith S. Briskin/SKS Foundation NeuroNetwork Emerging Scholar Fund (to Sarah E. Elzinga); the Handleman Emerging Scholar Fund (to Kevin S. Chen); the Tauber Family Student Internship Program (to Adam M. Allouch); the Taubman Foundation (to Eva L. Feldman); and the NeuroNetwork for Emerging Therapies (to Eva L. Feldman). Funding sources were not involved in the study design, collection, analysis, and interpretation of data, in the writing of the report, or in the decision to submit the article for publication. All living participants completed a donation pre-registration consent form. A verbal consent for autopsy from the participant's next of kin was obtained through our Michigan Medicine autopsy consent line.

CONFLICT OF INTEREST STATEMENT

The authors declare no conflicts of interest. Author disclosures are available in the supporting information.

DATA AVAILABILITY STATEMENT

AMP-AD data (single-nucleus RNA-seq; raw and processed data with sample processing, library preparation and sequencing, and primary processing methods and information) are available via the AD Knowledge Portal (https://adknowledgeportal.org). The AD Knowledge Portal is a platform for accessing data, analyses, and tools generated by the Accelerating Medicines Partnership (AMP-AD) Target Discovery Program and other National Institute on Aging (NIA)-supported programs to enable open-science practices and accelerate translational learning. The data, analyses, and tools are shared early in the research cycle without a publication embargo on secondary use. Data are available for general research use according to the following requirements for data access and data attribution (https://adknowledgeportal.synapse.org/Data%20Access). For access to AMP-AD content described in this manuscript see: https://doi.org/10.7303/syn2580853

ORCID

Sarah E. Elzinga https://orcid.org/0000-0002-4219-2712

REFERENCES

1. Zhang X-X, Tian Y, Wang Z-T, Ma Y-H, Tan L, Yu J-T. The epidemiology of Alzheimer's disease modifiable risk factors and prevention. *J Prev Alzheimers Dis*. 2021;8:313-321.
2. Tahami Monfared AA, Byrnes MJ, White LA, Zhang Q. Alzheimer's disease: epidemiology and clinical progression. *Neurol Ther*. 2022;11:553-569.
3. Blüher M. Obesity: global epidemiology and pathogenesis. *Nat Rev Endocrinol*. 2019;15(5):288-298.
4. Palmer MK, Toth PP. Trends in lipids, obesity, metabolic syndrome, and diabetes mellitus in the United States: an NHANES analysis (2003-2004 to 2013-2014). *Obesity*. 2019;27:309-314.
5. Hirode G, Wong RJ. Trends in the prevalence of metabolic syndrome in the United States, 2011-2016. *JAMA*. 2020;323:2526-2528.
6. Morys F, Dadar M, Dagher A. Association between midlife obesity and its metabolic consequences, cerebrovascular disease, and cognitive decline. *J Clin Endocrinol Metab*. 2021;106:e4260-e4274.
7. Hassing LB, Dahl AK, Pedersen NL, Johansson B. Overweight in midlife is related to lower cognitive function 30 years later: a prospective study with longitudinal assessments. *Dement Geriatr Cogn Disord*. 2010;29:543-552.
8. Savelieff MG, Chen KS, Elzinga SE, Feldman EL. Diabetes and dementia: clinical perspective, innovation, knowledge gaps. *J Diabetes Complications*. 2022;36(11):108333.
9. Henn RE, Noureldein MH, Elzinga SE, Kim B, Savelieff MG, Feldman EL. Glial-neuron crosstalk in health and disease: a focus on metabolism, obesity, and cognitive impairment. *Neurobiol Dis*. 2022;170:105766.
10. Biessels GJ, Despa F. Cognitive decline and dementia in diabetes mellitus: mechanisms and clinical implications. *Nat Rev Endocrinol*. 2018;14(10):591-604.
11. Van Eldik LJ, Carrillo MC, Cole PE, et al. The roles of inflammation and immune mechanisms in Alzheimer's disease. *Alzheimer's Dement Transl Res Clin Interv*. 2016;2(2):99-109.
12. Zhang W, Xiao D, Mao Q, Xia H. Role of neuroinflammation in neurodegeneration development. *Signal Transduct Target Ther*. 2023;8:267.

13. Scheiblich H, Trombly M, Ramirez A, Heneka MT. Neuroimmune connections in aging and neurodegenerative diseases. *Trends Immunol*. 2020;41:300-312.
14. Milanski M, Degasperi G, Coope A, et al. Saturated fatty acids produce an inflammatory response predominantly through the activation of TLR4 signaling in hypothalamus: implications for the pathogenesis of obesity. *J Neurosci*. 2009;29:359-370.
15. Qian X-H, Liu X-L, Chen S-D, Tang H-D. Integrating peripheral blood and brain transcriptomics to identify immunological features associated with Alzheimer's disease in mild cognitive impairment patients. *Front Immunol*. 2022;13:986346.
16. Poh L, Sim WL, Jo D-G, et al. The role of inflammasomes in vascular cognitive impairment. *Mol Neurodegener*. 2022;17:1-28.
17. Lehnardt S, Massillon L, Follett P, et al. Activation of innate immunity in the CNS triggers neurodegeneration through a Toll-like receptor 4-dependent pathway. *Proc Natl Acad Sci*. 2003;100:8514-8519.
18. Li Q, Zhao Y, Guo H, et al. Impaired lipophagy induced-microglial lipid droplets accumulation contributes to the buildup of TREM1 in diabetes-associated cognitive impairment. *Autophagy*. 2023;19:2639-2656.
19. de Paiva Lopes K, Yu L, Shen X, et al. Associations of cortical SPP1 and ITGAX with cognition and common neuropathologies in older adults. *Alzheimers Dement*. 2024;20:525-537.
20. De Schepper S, Ge JZ, Crowley G, et al. Perivascular cells induce microglial phagocytic states and synaptic engulfment via SPP1 in mouse models of Alzheimer's disease. *Nat Neurosci*. 2023;26(3):406-415.
21. Butler MJ, Cole RM, Deems NP, Belury MA, Barrientos RM. Fatty food, fatty acids, and microglial priming in the adult and aged hippocampus and amygdala. *Brain Behav Immun*. 2020;89:145-158.
22. Cope EC, LaMarca EA, Monari PK, et al. Microglia play an active role in obesity-associated cognitive decline. *J Neurosci*. 2018;38:8889-8904.
23. Hansen DV, Hanson JE, Sheng M. Microglia in Alzheimer's disease. *J Cell Biol*. 2018;217:459-472.
24. Elzinga SE, Henn R, Murdock BJ, et al. cGAS/STING and innate brain inflammation following acute high-fat feeding. *Front Immunol*. 2022;13:1012594.
25. Valdearcos M, Douglass JD, Robblee MM, et al. Microglial inflammatory signaling orchestrates the hypothalamic immune response to dietary excess and mediates obesity susceptibility. *Cell Metab*. 2017;26:185-197.e183.
26. Wang C, Li H, Chen C, et al. High-fat diet consumption induces neurobehavioral abnormalities and neuronal morphological alterations accompanied by excessive microglial activation in the medial prefrontal cortex in adolescent mice. *Int J Mol Sci*. 2023;24:9394.
27. Wu M, Liao M, Huang R, et al. Hippocampal overexpression of TREM2 ameliorates high fat diet induced cognitive impairment and modulates phenotypic polarization of the microglia. *Genes Dis*. 2022;9(2):401-414.
28. Wang W-Y, Tan M-S, Yu J-T, Tan L. Role of pro-inflammatory cytokines released from microglia in Alzheimer's disease. *Ann Transl Med*. 2015;3(10):136.
29. Hinder LM, O'Brien PD, Hayes JM, et al. Dietary reversal of neuropathy in a murine model of prediabetes and metabolic syndrome. *Dis Model Mech*. 2017;10(6):717-725.
30. Elzinga SE, Koubek EJ, Hayes JM, et al. Modeling the innate inflammatory cGAS/STING pathway: sexually dimorphic effects on microglia and cognition in obesity and prediabetes. *Front Cell Neurosci*. 2023;17:1167688.
31. Henn RE, Elzinga SE, Glass E, et al. Obesity-induced neuroinflammation and cognitive impairment in young adult versus middle-aged mice. *Immun Ageing*. 2022;19(1):67.
32. McGinley LM, Kashlan ON, Bruno ES, et al. Human neural stem cell transplantation improves cognition in a murine model of Alzheimer's disease. *Sci Rep*. 2018;8:14776.
33. York EM, Ledue JM, Bernier LP, Macvicar BA. 3dmorph automatic analysis of microglial morphology in three dimensions from ex vivo and in vivo imaging. *eNeuro*. 2018;5(6). doi:10.1523/ENEURO.0266-18.2018
34. Guo K, Eid SA, Elzinga SE, Pacut C, Feldman EL, Hur J. Genome-wide profiling of DNA methylation and gene expression identifies candidate genes for human diabetic neuropathy. *Clin Epigenetics*. 2020;12(1):123.
35. Gehring TV, Luksys G, Sandi C, Vasilaki E. Detailed classification of swimming paths in the Morris Water Maze: multiple strategies within one trial. *Sci Rep*. 2015;5:14562.
36. Vouros A, Gehring TV, Szydlowska K, et al. A generalised framework for detailed classification of swimming paths inside the Morris Water Maze. *Sci Rep*. 2018;8:15089.
37. Zeisel A, Hochgerner H, Lönnerberg P, et al. Molecular architecture of the mouse nervous system. *Cell*. 2018;174:999-1014.e1022.
38. Jin S, Guerrero-Juarez CF, Zhang L, et al. Inference and analysis of cell-cell communication using CellChat. *Nat Commun*. 2021;12:1088.
39. Ben Abdallah NM, Fuss J, Trusel M, et al. The puzzle box as a simple and efficient behavioral test for exploring impairments of general cognition and executive functions in mouse models of schizophrenia. *Exp Neurol*. 2011;227(1):42-52.
40. Antal B, McMahon LP, Sultan SF, et al. Type 2 diabetes mellitus accelerates brain aging and cognitive decline: complementary findings from UK Biobank and meta-analyses. *eLife*. 2022;11:e73138.
41. Sims-Robinson C, Bakeman A, Bruno E, et al. Dietary reversal ameliorates short-and long-term memory deficits induced by high-fat diet early in life. *PLoS One*. 2016;11:e0163883.
42. Zhuang H, Yao X, Li H, et al. Long-term high-fat diet consumption by mice throughout adulthood induces neurobehavioral alterations and hippocampal neuronal remodeling accompanied by augmented microglial lipid accumulation. *Brain Behav Immun*. 2022;100:155-171.
43. Fonseca MI, Chu S-H, Hernandez MX, et al. Cell-specific deletion of C1qa identifies microglia as the dominant source of C1q in mouse brain. *J Neuroinflam*. 2017;14:1-15.
44. Beg AA, Ruben SM, Scheinman RI, Haskill S, Rosen CA. I kappa B interacts with the nuclear localization sequences of the subunits of NF-kappa B: a mechanism for cytoplasmic retention. *Genes Dev*. 1992;6(10):1899-1913.
45. Scherer DC, Brockman JA, Chen Z, Maniatis T, Ballard DW. Signal-induced degradation of I kappa B alpha requires site-specific ubiquitination. *Proc Natl Acad Sci*. 1995;92:11259-11263.
46. Pistell PJ, Morrison CD, Gupta S, et al. Cognitive impairment following high fat diet consumption is associated with brain inflammation. *J Neuroimmunol*. 2010;219:25-32.
47. Wang Z, Ge Q, Wu Y, Zhang J, Gu Q, Han J. Impairment of long-term memory by a short-term high-fat diet via hippocampal oxidative stress and alterations in synaptic plasticity. *Neuroscience*. 2020;424:24-33.
48. de Paula GC, Brunetta HS, Engel DF, et al. Hippocampal function is impaired by a short-term high-fat diet in mice: increased blood–brain barrier permeability and neuroinflammation as triggering events. *Front Neurosci*. 2021;15:734158.
49. Ghannam N, Alahmed S, Aldahash R, et al. Addressing the continuum of dysglycaemia and vascular complications in prediabetes and type 2 diabetes: need for early and intensive treatment. *Diabetes Metab Syndr Obes*. 2023;16:105-115.
50. Luchsinger JA. The relationship between the continuum of elevated adiposity, hyperinsulinemia, and type 2 diabetes and late-onset Alzheimer's disease: an epidemiological perspective. In: Craft S, Christen Y, eds. *Diabetes, Insulin and Alzheimer's Disease. Research and Perspectives in Alzheimer's Disease*. Springer; 2010. doi:10.1007/978-3-642-04300-0_7
51. Biessels GJ, Strachan MW, Visseren FL, Kappelle LJ, Whitmer RA. Dementia and cognitive decline in type 2 diabetes and prediabetic stages: towards targeted interventions. *Lancet Diabetes Endocrinol*. 2014;2:246-255.

52. Madduma Hewage S, Prashar S, Debnath SC, Karmin O, Siow YL. Inhibition of inflammatory cytokine expression prevents high-fat diet-induced kidney injury: role of lingonberry supplementation. *Front Med*. 2020;7:80.
53. Ding X, Jian T, Li J, et al. Chicoric acid ameliorates nonalcoholic fatty liver disease via the AMPK/Nrf2/NFκB signaling pathway and restores gut microbiota in high-fat-diet-fed mice. *Oxid Med Cell Long*. 2020;2020:9734560.
54. van der Heijden RA, Sheedfar F, Morrison MC, et al. High-fat diet induced obesity primes inflammation in adipose tissue prior to liver in C57BL/6j mice. *Aging (Albany NY)*. 2015;7:256.
55. Nimmerjahn A, Kirchhoff F, Helmchen F. Resting microglial cells are highly dynamic surveillants of brain parenchyma in vivo. *Science*. 2005;308:1314-1318.
56. Cătălin B, Stopper L, Bălşeanu T-A, Scheller A. The in situ morphology of microglia is highly sensitive to the mode of tissue fixation. *J Chem Neuroanat*. 2017;86:59-66.
57. Godeanu S, Clarke D, Stopper L, et al. Microglial morphology in the somatosensory cortex across lifespan. A quantitative study. *Dev Dyn*. 2023;252:1113-1129.
58. de Carvalho Borges B, Rorato R, Uchoa ET, et al. High-fat diet induces site-specific unresponsiveness to LPS-stimulated STAT3 activation in the hypothalamus. *Am J Physiol-Regul, Integr Comp Physiol*. 2014;306:R34-R44.
59. Frasca D, Blomberg BB, Paganelli R. Aging, obesity, and inflammatory age-related diseases. *Front Immunol*. 2017;8:1745.
60. Schafer MJ, Zhang X, Kumar A, et al. The senescence-associated secretome as an indicator of age and medical risk. *JCI Insight*. 2020;5(12):e133668.
61. Behfar Q, Ramirez Zuniga A, Martino-Adami PV. Aging, senescence, and dementia. *J Prev Alzheimers Dis*. 2022;9(3):523-531.
62. Kumari R, Jat P. Mechanisms of cellular senescence: cell cycle arrest and senescence associated secretory phenotype. *Front Cell Dev Biol*. 2021;9:485.
63. Angelova DM, Brown DR. Microglia and the aging brain: are senescent microglia the key to neurodegeneration? *J Neurochem*. 2019;151:676-688.
64. Kwon HS, Koh S-H. Neuroinflammation in neurodegenerative disorders: the roles of microglia and astrocytes. *Transl Neurodegener*. 2020;9:42.
65. Bartels T, De Schepper S, Hong S. Microglia modulate neurodegeneration in Alzheimer's and Parkinson's diseases. *Science*. 2020;370:66-69.
66. Yim A, Smith C, Brown AM. Osteopontin/secreted phosphoprotein-1 harnesses glial-, immune-, and neuronal cell ligand-receptor interactions to sense and regulate acute and chronic neuroinflammation. *Immunol Rev*. 2022;311:224-233.
67. Lin EY-H, Xi W, Aggarwal N, Shinohara ML. Osteopontin (OPN)/SPP1: from its biochemistry to biological functions in the innate immune system and the central nervous system (CNS). *Int Immunol*. 2023;35:171-180.
68. Sankowski R, Böttcher C, Masuda T, et al. Mapping microglia states in the human brain through the integration of high-dimensional techniques. *Nat Neurosci*. 2019;22:2098-2110.
69. Shinohara ML, Jansson M, Hwang ES, Werneck MBF, Glimcher LH, Cantor H. T-bet-dependent expression of osteopontin contributes to T cell polarization. *Proc Natl Acad Sci*. 2005;102:17101-17106.
70. Shinohara ML, Lu L, Bu J, et al. Osteopontin expression is essential for interferon-α production by plasmacytoid dendritic cells. *Nat Immunol*. 2006;7:498-506.
71. Inoue M, Arikawa T, Chen Y-H, et al. T cells down-regulate macrophage TNF production by IRAK1-mediated IL-10 expression and control innate hyperinflammation. *Proc Natl Acad Sci*. 2014;111:5295-5300.
72. Inoue M, Moriwaki Y, Arikawa T, et al. Cutting edge: critical role of intracellular osteopontin in antifungal innate immune responses. *J Immunol*. 2011;186:19-23.
73. Chai YL, Chong JR, Raquib AR, et al. Plasma osteopontin as a biomarker of Alzheimer's disease and vascular cognitive impairment. *Sci Rep*. 2021;11:4010.
74. Tramunt B, Smati S, Grandgeorge N, et al. Sex differences in metabolic regulation and diabetes susceptibility. *Diabetologia*. 2020;63:453-461.
75. Elzinga SE, Savelieff MG, O'Brien PD, Mendelson FE, Hayes JM, Feldman EL. Sex differences in insulin resistance, but not peripheral neuropathy, in a diet-induced prediabetes mouse model. *Dis Model Mech*. 2021;14(4):dmm048909.
76. Meneses G, Rosetti M, Espinosa A, et al. Recovery from an acute systemic and central LPS-inflammation challenge is affected by mouse sex and genetic background. *PLoS One*. 2018;13:e0201375.
77. Zore T, Palafox M, Reue K. Sex differences in obesity, lipid metabolism, and inflammation-A role for the sex chromosomes? *Mol Metab*. 2018;15:35-44.

SUPPORTING INFORMATION

Additional supporting information can be found online in the Supporting Information section at the end of this article.

How to cite this article: Elzinga SE, Guo K, Turfah A, et al. Metabolic stress and age drive inflammation and cognitive decline in mice and humans. *Alzheimer's Dement*. 2025;21:e70060. https://doi.org/10.1002/alz.70060